Supporting information

Azacalixphyrins as NIR Photoacoustic Contrast Agents

Lucien Lavaud,[a] Simon Pascal,*[a] Khaled Metwally,[b] Damien Gasteau,[b] Anabela Da Silva,*[b] Zhongrui Chen,[a] Mourad Elhabiri,[c] Gabriel Canard,[a] Denis Jacquemin[d] and Olivier Siri*[a]

a. Aix-Marseille Université, CNRS UMR 7325, Centre Interdisciplinaire de Nanoscience de Marseille (CINaM), Campus de Luminy, 13288 Marseille cedex 09, France.

b. Aix-Marseille Université, CNRS, Institut Fresnel, F-13013 Marseille, France.

c. Université de Strasbourg, Université de Haute-Alsace, CNRS, LIMA, UMR 7042, Equipe Chimie Bioorganique et Médicinale, ECPM, 25 Rue Becquerel, 67000 Strasbourg, France.

d. Laboratoire CEISAM, CNRS UMR 6230, Université de Nantes, 2, rue de la Houssinière, 44322 Nantes, France.

TABLE OF CONTENT

S-I. GENERAL REMARKS AND ANALYSIS CONDITIONS 2

S-II. SYNTHETIC PROTOCOLS AND CHARACTERIZATIONS 4

S-III. ^{1}H AND ^{13}C NMR SPECTRA 10

S-I. ELECTRONIC ABSORPTION AND TITRATIONS 21

S-II. PHOTOACOUSTIC 26

S-III. THEORETICAL MODELLING 29

S-IV. REFERENCES 33

S-I. GENERAL REMARKS AND ANALYSIS CONDITIONS

Analytical methods and apparatus. NMR spectra were recorded on a JEOL ECS400 NMR spectrometer at room temperature. NMR chemical shifts are given in ppm (δ) relative to Me_4Si with solvent resonances used as internal standards ($CDCl_3$: 7.26 ppm for ^1H and 77.2 for ^{13}C; Acetone-d_6: 2.05 ppm for ^1H and 29.8 for ^{13}C; DMSO-d_6: 2.50 ppm for ^1H and 39.5 for ^{13}C). UV-Vis-NIR absorption spectra were recorded on a VARIAN CARY 50 SCAN spectrophotometer at room temperature. HRMS (ESI) and MS (ESI) analyses were performed on a QStar Elite (Applied Biosystems SCIEX) or a SYNAPT G2 HDMS (Waters) spectrometers by the "*Spectropole*" of the Aix-Marseille University. These two instruments were equipped with an ESI or MALDI source spectrometer.

Starting Materials and Solvents. Distilled water was further purified by passing it through a mixed bed of ion-exchanger (Bioblock Scientific R3-83002, M3-83006) and activated carbon (Bioblock Scientific ORC-83005). Spectrophotometric grade methanol (Merck, p.a.) and water were de-oxygenated by CO_2- and O_2-free argon (Sigma Oxiclear cartridge) before use. All the stock solutions were prepared by weighing solid products using an AG 245 Mettler Toledo analytical balance (precision 0.01 mg). The ionic strength was maintained at 0.1 M with *n*-tetrabutylammonium perchlorate (NBu_4ClO_4, Fluka, puriss), and all measurements were carried out at 25.0(2) °C by the flow of a Lauda E200 thermostat. *CAUTION! Perchlorate salts combined with organic ligands are potentially explosive and should be handled in small quantities and with the adequate precautions*.[1]

Potentiometric and UV-Vis titrations. A stock solution of **3a** (2.99×10^{-3} M) was first prepared by quantitative dissolution of a solid sample in methanol. The **3a** solution (2.19×10^{-5} M) was then diluted in CH_3OH/H_2O solvent (80/20 *w/w*) containing the supporting electrolyte at 0.1 M (NBu_4ClO_4, Fluka, puriss). An aliquot of 40 mL was then introduced into a jacketed cell (Metrohm) maintained at 25.0 ± 0.2 °C by the flow of a Lauda E200 thermostat. The free hydrogen ion concentrations were measured with a combined glass electrode (Metrohm 6.0234.500, Long Life) and an automatic titrator system 794 Basic Titrino (Metrohm) connected to a microcomputer (Tiamo light 1.2 program for the acquisition of the potentiometric data).The Ag/AgCl reference electrode was filled with 0.1 M NaCl (Fluka, p.a.) in $MeOH/H_2O$ (80/20 *w/w*). Prior to the absorption *versus* pH titration, the combined glass electrode was calibrated as a hydrogen concentration probe by titrating known amounts of perchloric acid (~10^{-1} M from $HClO_4$, Prolabo, normapur, 70% min) with CO_2-free *n*-tetrabutylammonium hydroxide solution (~10^{-1} M from Fluka, purum, ~40 % in water).[2] The $HClO_4$ and NBu_4OH solutions were freshly prepared just before use in CH_3OH/H_2O solvent and their analytical concentrations were ascertained by colorimetric titrations with sodium tetraborate decahydrate ($B_4Na_2O_7.10H_2O$, Fluka, puriss, p.a.) and potassium hydrogen phthalate ($C_8H_5KO_3$, Fluka, puriss, p.a.), respectively, using methyl orange (RAL) and phenolphthalein (Prolabo, purum) as the indicators. The GLEE program was applied for the glass electrode calibration and to check carbonate levels of the NBu_4OH solutions used (< 5%).

The initial pH of the **3a** solution was adjusted to ~2.4 with $HClO_4$ (Prolabo, normapur, 70% min), and duplicated titrations of **3a** (~2.4 < pH < ~11.5) were then carried out (Figure S21) by adding known

volumes of NBu_4OH solutions with the automatic titrator (794 Basic Titrino device). After each addition of base, an absorption spectrum was automatically recorded using a Varian CARY 50 spectrophotometer fitted with Hellma optical fibres (Hellma, 041.002-UV) and an immersion probe made of quartz suprazil (Hellma, 661.500-QX) that was interfaced (Cetrib) with the potentiometric unit (794 Basic Titrino device) (*i.e.,* the volumes and thereby the pH increments along the absorption *vs*. pH titrations were automatically adjusted by the potentiometric system according the signal drift of the solution. The DET - Dynamic Potential Titration - method of the Tiamo program was used with a measuring point density of 3).

Refinement of the titration data. The absorption spectrophotometric and potentiometric data were analysed with the Specfit[3] program that adjusts the absorptivities and the stability constants of the species formed at equilibrium. Specfit uses factor analysis to reduce the absorbance matrix and to extract the eigenvalues prior to the multi-wavelength fit of the reduced data set according to the Marquardt algorithm.[4] The distribution curves of the protonated species of **3a** as a function of pH were calculated using the Hyss program.[5]

Photoacoustic measurements. An experimental setup was built using a high energy (up to 120 mJ, 20Hz) NIR range tuneable laser (Ekspla NT350) with an integrated Optical Parametric Oscillator (OPO) system (pumped by Nd:YAG), that allows a broad tuning range of 670-2600 nm. The free-space laser beam was directed, through a high power optical fibre (MHP910L02, Ø 910 µm Core, 0.22 NA, Thorlabs) with an output collimater (Ø 1.2 mm), to a custom-made optoacoustic combiner (transparent gel from Clear ballistics) that allows performing the samples measurement under the reflection geometry. It has to combine a high level of transparency in the optical illumination path and a high reflectivity for the epi-detection of the acoustic waves. The measuring head was mounted on a Cartesian micro-manipulator to ensure scanning of the zone of interest (Figure S26). In order to avoid boundary effects of the cylindrical tube, a volume of 10 ml of the samples were introduced in an OptiCell™ chamber (Thermo Fisher Scientific), made up of two thin, flexible and transparent, polystyrene membranes (thickness: 80 µm, distance between membranes: 2mm). The equation describing the generated pressure: $P_0 = \Gamma\mu_a(\lambda)\varphi(\lambda)$, with Γ [dimensionless] the Grueneisen coefficient, depending on the acoustic properties of the propagating medium; $\varphi(\lambda) = \varphi(\mu_a(\lambda), \mu_s'(\lambda))$ is the optical fluence [W.m^{-2}] depending on the optical properties of the probed medium, essentially $\mu_a(\lambda)$ (resp. $\mu_s'(\lambda)$, to be considered if scattering media) is the absorption (resp. reduced scattering) coefficient [m^{-1}] as a function of the wavelength. For the scanning of the soft transparent tube, a calibration protocol was adopted in order to account for the instrument response function. Finally, a post-processing correction of background effects was applied by subtracting acquired measurements on the tubes filled with the solvents (MeOH, DMSO) from those performed on the tubes filled with the studied solutions. As the measurements were performed under the reflection geometry, the samples are probed at depth z = 0. As a result, the post-processed signal P is directly proportional to the absorption coefficient of the molecules present in the tubes at a given concentration: $P = \Gamma\mu_{a,ACPs}(\lambda)\varphi_0(\lambda) \propto \mu_{a,ACPs}(\lambda)$ where $\mu_{a,ACPs}$ is the absorption of the ACP molecule.

S-II. SYNTHETIC PROTOCOLS AND CHARACTERIZATIONS

Reagents All reagents were purchased from Alfa-Aesar and used as received. Column chromatography were performed using Silica 60M (0.04-0.063 mm) purchased from Macherey-Nagel and alumina (Neutral, Brockmann activity I) purchased from Merck. Compounds **5a-b**[6] were prepared following previously reported protocols.

Synthesis of N^1,N^3-bis(3-(trifluoromethyl)phenyl)-4,6-dinitrobenzene-1,3-diamine (4c)

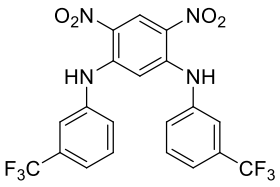

A mixture of 1,5-difluoro-2,4-dinitrobenzene (5.00 g, 24.4 mmol, 1 equiv.), 3-(trifluoromethyl)aniline (5.9 mL, 51.2 mmol, 2.1 equiv.) and *N,N*-diisopropylethylamine (25 mL, 144 mmol, 6 equiv.) was heated at 140 °C for 2 hours in a pressure tube. The reaction mixture was then cooled to room temperature and the resulting precipitate was filtered, washed with ethanol and dried under vacuum to afford the product as an orange solid (10.41 g, 2.1 mmol, 86%). **^{1}H NMR (400 MHz, DMSO-d_6):** δ = 9.89 (br s, 2H, NH), 9.05 (s, 1H, ArH), 7.66 – 7.50 (m, 8H, ArH), 6.29 (s, 1H, ArH). **^{13}C NMR (100 MHz, DMSO-d_6):** δ = 145.7, 138.9, 130.3, 130.2 (q, $^2J_{FC}$ = 32 Hz), 128.6, 128.1, 126.6, 126.6 (q, $^1J_{FC}$ = 273 Hz), 122.3, 121.64, 96.80. **HRMS (ESI-TOF):** calcd for $C_{20}H_{13}N_4O_4F_6^+$ ([M + H]$^+$) 487.0836, found 487.0836.

Synthesis of N^1,N^5-bis(3-(trifluoromethyl)phenyl)-benzene-1,2,4,5-tetraamine dihydrochloride (5c)

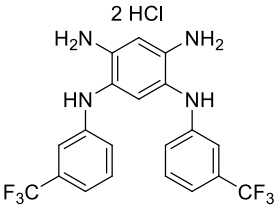

A solution of **4c** (2.00 g, 4.11 mmol, 1 equiv.) and $SnCl_2{\cdot}2H_2O$ (12.84 g, 33 mmol, 8 equiv.) in aqueous HCl (12 N, 25 mL) and DCM (25 mL) was placed in a pressure bomb closed with a Teflon seal. The mixture was stirred at 50 °C for 4 days. The resulting solid was filtered, washed successively with aqueous HCl (12 N) and Et_2O before being dried under vacuum to afford the product as a light green powder (1.14 g, 2.3 mmol, 55%). **^{1}H NMR (400 MHz, DMSO-d_6):** δ = 8.79 (br s, 2H, NH), 7.49 (s, 1H, ArH), 7.41 (t, 2H, $^3J_{HH}$ = 7.9 Hz, ArH), 7.24 – 7.11 (m, 7H, ArH). No ^{13}C NMR was recorded due to the fast degradation of **5c**. **HRMS (MALDI-TOF):** calcd for $C_{20}H_{16}N_4F_6^{+\bullet}$ ([M]$^{+\bullet}$) 426.1274, found 426.1274.

Synthesis of N^1,N^5-bis(5-fluoro-2,4-dinitrophenyl)-N^2,N^4-bis(3,4,5-trimethoxyphenyl)benzene-1,2,4,5-tetraamine (6a)

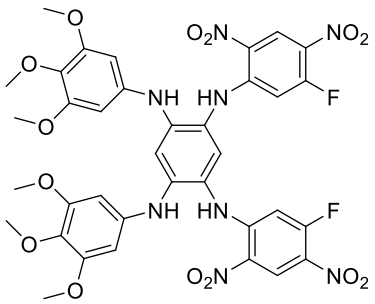

To a solution of 1,5-difluoro-2,4-dinitrobenzene (135 mg, 0.66 mmol, 1.8 equiv.) in anhydrous and degassed MeCN (40 mL), was added **5a** (200 mg, 0.37, 1.0 equiv.) under argon atmosphere. Then degassed DIPEA (513 µL, 5.28 mmol, 8.0 equiv.) was added dropwise at 0 °C. The solution was stirred at 0 °C for 4 hours and then at room temperature overnight. After evaporation of the solvent, the resulting solid was washed with EtOH to afford the product as a brown powder (265 mg, 0.316 mmol, 96%).

^{1}H NMR (400 MHz, $CDCl_3$): δ = 9.45 (br s, 2H, NH), 9.08 (d, $^4J_{HF}$ = 7.6 Hz, 2H, ArH), 7.14 (s, 1H, ArH), 7.10 (s, 1H, ArH), 6.68 (d, $^3J_{HF}$ = 13.2 Hz, 2H, ArH), 6.29 (s, 4H, ArH), 5.88 (br s, 2H, NH), 3.78 (s, 6H, OCH_3), 3.72 (s, 12H, OCH_3). **^{13}C NMR (100 MHz, $CDCl_3$):** δ = 161.2 (d, $^1J_{FC}$ = 271 Hz), 153.8, 149.3, 149.1, 143.1, 135.7, 135.2, 128.2, 128.1, 127.6, 127.5 (d, $^2J_{FC}$ = 10 Hz), 114.3, 103.8 (d, $^2J_{FC}$ = 28 Hz), 100.3, 100.2, 61.0, 56.2. **HRMS (ESI-TOF):** calcd for $C_{36}H_{36}N_9O_{14}F_2^+$ $[M+NH_4]^+$ 856.2344, found 856.2349. **TLC:** Silica F60, DCM/EtOAc (90/10), Rf = 0.52.

Synthesis of N^1,N^5-bis(5-fluoro-2,4-dinitrophenyl)-N^2,N^4-bis(4-tertbutylpnenyl)benzene-1,2,4,5-tetraamine (6b)

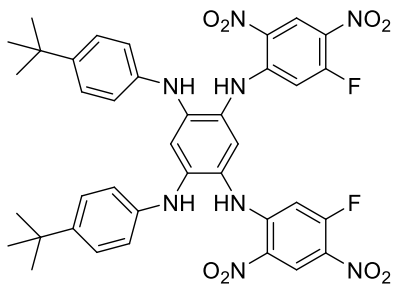

To a solution of 1,5-difluoro-2,4-dinitrobenzene (0.86 g, 4.2 mmol, 2.0 equiv.) in degassed MeCN (200 mL), was added **5b** (1.00 g, 2.1 mmol, 1.0 equiv.) under argon atmosphere. Then degassed DIPEA (2.19 mL, 6.0 equiv.) was added dropwise at 0 °C. The solution was stirred at 0 °C for 1 hour and then at room temperature overnight. After evaporation of the solvent, the resulting solid was washed with EtOH to afford the product as a brown powder (0.90 g, 1.16 mmol, 56%).

^{1}H NMR (400 MHz, $CDCl_3$): δ = 9.82 (br s, 2H), 8.89 (d, $^4J_{HF}$ = 8 Hz, 2H), 7.72 (s, 2H), 7.26 (d, $^3J_{HH}$ = 8.7 Hz, 4H), 7.16 (s, 1H), 7.03 (d, $^3J_{HH}$ = 8.7 Hz, 4H), 7.00 (s, 1H), 6.89 (d, $^3J_{HF}$ = 14.4 Hz, 2H), 1.22 (s, 18H). **^{13}C NMR (100 MHz, $CDCl_3$):** δ = 158.6 (d, $^1J_{FC}$ = 265 Hz), 149.2 (d, $^2J_{FC}$ = 11 Hz), 144.0, 141.0, 139.1, 128.5, 128.0, 126.8, 125.6, 125.5, 119.9, 115.7, 103.3 (d, $^2J_{FC}$ = 28 Hz), 102.2, 33.8, 31.1. **HRMS (ESI-TOF):** calcd. for $C_{38}H_{37}N_8O_8F_2^+$ ($[M+H]^+$) 771.2697, found 771.2700.

Synthesis of N^1,N^5-bis(5-fluoro-2,4-dinitrophenyl)-N^2,N^4-bis(4-(trifluoromethyl)phenyl)benzene-1,2,4,5-tetraamine (6c)

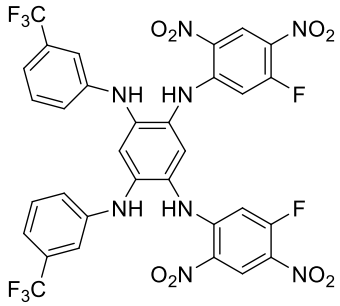

To a solution of 1,5-difluoro-2,4-dinitrobenzene (2.25 g, 11 mmol, 2.2 equiv.) in degassed MeCN (200 mL), was added **5c** (2.50 g, 5 mmol, 1 equiv.) under argon atmosphere. Then degassed DIPEA (6.94 mL, 8 equiv.) was added dropwise at 0 °C. The solution was stirred at 0 °C overnight and then at room temperature for 1 day. After evaporation of the solvent, the resulting solid was purified by column chromatography (silica F60, DCM:cyclohexane, 8/2 to 10/0) to afford the desired the product as a yellow solid (1.40 g, 1.7 mmol, 35%).

^{1}H NMR (400 MHz, $CDCl_3$): δ = 9.89 (br s, 2H, NH), 8.89 (d, $^4J_{HF}$ = 7.9 Hz, 2H, ArH), 8.17 (s, 2H), 7.49 – 7.39 (m, 4H, ArH), 7.33 (s, 1H, ArH), 7.3 (br s, 2H, ArH), 7.17 (br d, $^4J_{HF}$ = 7.1 Hz, ArH), 7.15 (s, 1H, ArH), 7.00 (d, $^3J_{HF}$ = 14.3 Hz, 2H, ArH). **^{13}C NMR (100 MHz, $CDCl_3$):** δ = 158.9 (d, $^1J_{FC}$ = 266 Hz), 148.8 (d, $^2J_{FC}$ = 13 Hz), 143.2, 139.2, 130.0, 129.9 (q, $^2J_{FC}$ = 32 Hz), 128.8, 128.0, 126.7, 126.1 (q, $^1J_{FC}$ = 272 Hz), 125.9 (d, $^2J_{FC}$ = 9 Hz), 121.6, 120.0, 119.5, 117.0, 114.6, 106.5, 103.9, 103.8 (d, $^2J_{FC}$ = 28 Hz). **HRMS (ESI-TOF):** calcd. for $C_{32}H_{19}N_8O_8F_8^+$ ($[M+NH_4]^+$) 812.1458, found 812.1463. **TLC**: Silica F60, DCM/cyclohexane (80/20), Rf = 0.16.

Synthesis of tetrakis(3,4,5-trimethoxyphenyl) azacalix[4]arene (7a)

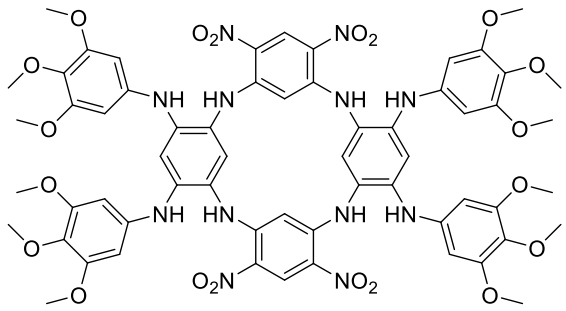

To a solution of **6a** (600 mg, 0.715 mmol, 1 equiv.) in anhydrous and degassed MeCN (65 mL), was added **5a** (555 g, 1.022 mmol, 1.4 equiv.) under argon atmosphere. Then degassed DIPEA (1.42 mL, 8.18 mmol, 8 equiv.) was added dropwise at 0 °C. The solution was stirred for 3 hours at room temperature and then heated to reflux overnight. After evaporation of the solvent, the resulting solid was purified by alumina column chromatography (DCM:acetone, 8.5/1.5 to 7/3) to afford the desired product as an orange powder (0.441 g, 0.347 mmol, 49%).

^{1}H NMR (400 MHz, Acetone-d_6): δ = 9.17 (s, 2H, ArH), 9.09 (br s, 4H, NH), 7.15 (s, 2H, ArH), 6.91 (s, 2H, ArH), 6.20 (s, 8H, ArH), 6.01 (br s, 4H, NH), 5.85 (s, 2H, ArH), 3.75 (s, 12H, OCH_3), 3.54 (s, 24H, OCH_3). **^{13}C NMR (100 MHz, Acetone-d_6):** δ = 158.3, 149.6, 143.0, 136.3, 134.9, 130.0, 129.0, 125.5, 114.9, 99.7, 98.8, 95.5, 60.9, 56.0. **HRMS (ESI-TOF):** calcd. for $C_{60}H_{62}N_{12}O_{20}^{2+}$ ($[M+2H]^{2+}$) 635.2096, found 635.2100. **TLC:** Silica F60, DCM/MeOH (96/4), Rf = 0.34.

Synthesis of tetrakis(4-tertbutylpnenyl) azacalix[4]arene (7b)

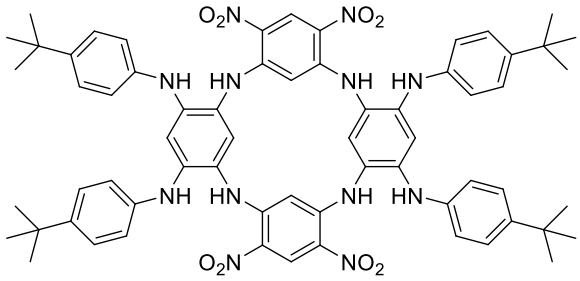

To a solution of **6b** (100 mg, 0.129 mmol, 1 equiv.) in degassed MeCN (30 mL), was added **5b** (92 mg, 0.194 mmol, 1.5 equiv.) under argon atmosphere. Then degassed DIPEA (180 µL, 1.032 mmol, 8 equiv.) was added dropwise at 0 °C. The solution was stirred for 3 hours at room temperature and finally heated to reflux overnight. After evaporation of the solvent, the resulting solid was washed with EtOH to afford the product as an orange powder (40 mg, 0.035 mmol, 27%).

^{1}H NMR (400 MHz, DMSO-*d*$_6$): δ = 9.11 (br s, 4H, NH), 8.99 (s, 2H, ArH), 7.63 (br s, 4H, NH), 7.14 (d, $^3J_{HH}$ = 8.5 Hz, ArH), 7.01 (s, 2H, ArH), 6.97 (d, $^3J_{HH}$ = 8.5 Hz, ArH), 6.88 (s, 2H, ArH), 5.85 (s, 2H, ArH), 1.19 (s, 36H, CH_3). The compound was too insoluble to record a ^{13}C NMR spectrum. **HRMS (ESI-TOF):** calcd. for $C_{64}H_{69}N_{12}O_8^+$ ([M+H]$^+$) 1133.5356, found 1133.5356.

Synthesis of tetrakis(4-(trifluoromethyl)phenyl) azacalix[4]arene (7c)

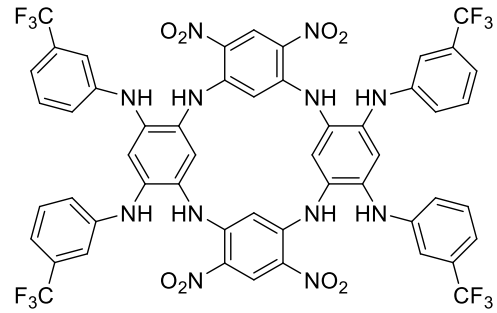

To a solution of **6c** (800 mg, 1 mmol, 1 equiv.) in degassed MeCN (100 mL), was added **5c** (754 mg, 1.5 mmol, 1.5 equiv.) under argon atmosphere. Then degassed DIPEA (1.39 mL, 8 mmol, 8 equiv.) was added dropwise at 0 °C. The solution was stirred for 2 hours at room temperature and finally heated to reflux overnight. After evaporation of the solvent, the resulting solid was washed with EtOH to obtain the desired product as an orange powder (624 mg, 0.53 mmol, 53%).

^{1}H NMR (400 MHz, DMSO-*d*$_6$): δ = 9.26 (s, 4H, NH), 9.04 (s, 2H, ArH), 7.95 (s, 4H, NH), 7.19 – 6.96 (m, 20H, ArH), 5.60 (s, 2H, ArH). The compound was too insoluble to record a ^{13}C NMR spectrum. **HRMS (ESI-TOF):** calcd. for $C_{52}H_{33}N_{12}O_8F_{12}^+$ ([M+H]$^+$) 1181.2347, found 1181.2345.

Synthesis of *N²,N⁴,N¹⁴,N¹⁶*-tetrakis(3,4,5-trimethoxylphenyl)-azacalixphyrin (3a)

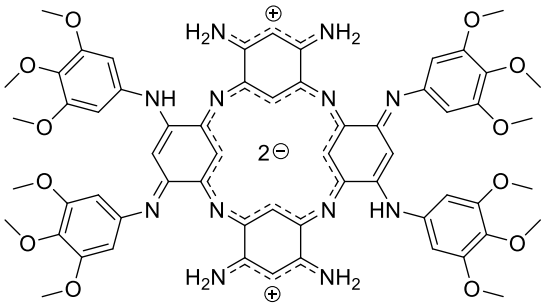

Compound **7a** (100 mg, 78.8 µmol, 1 equiv.), Pd on carbon 5% (40 mg, 18.7 µmol, 0.24 equiv.) and THF (40 mL) were introduced into a pressure bomb. Then hydrazine monohydrate (390 µL, 0.795 mmol, 100 equiv.) was added to the mixture before closing the bomb with a Teflon seal. The mixture was stirred at 100 °C for 30 hours. The resulting solution was diluted with MeOH (100 mL) before air was bubbled in the mixture at 40 °C for 24 hours. After evaporation of the solvent, the residue was purified on alumina column chromatography (DCM/MeOH 10/0 to 8/2) to afford the product as dark solid (40 mg, 3.50 µmol, 45%).

^{1}H NMR (400 MHz, CD_3OD): δ = 6.81 (s, 10H, ArH and CH), 6.38 (s, 2H, CH), 3.79 (s, 12H, OCH_3), 3.78 (s, 24H, OCH_3), –1.26 (s, 2H, ArH), -1.30 (s, 2H, ArH). Only incomplete ^{13}C NMR spectrum were recorded due to poorly resolved signals (Figure S15). **HRMS (ESI-TOF):** calcd. for $C_{60}H_{64}N_{12}O_{12}^{2+}$ ($[M+2H]^{2+}$) 572.2378, found 572.2379.

Synthesis of *N²,N⁴,N¹⁴,N¹⁶*-tetrakis(4-tertbutylpnenyl)-azacalixphyrin (3b)

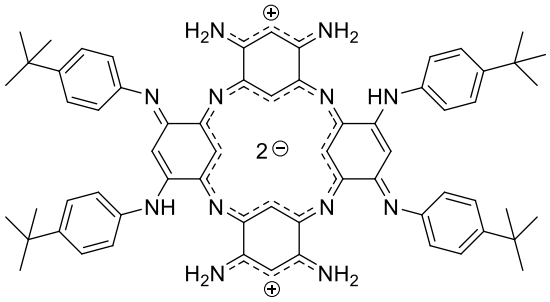

Compound **7b** (75 mg, 66.2 µmol, 1 equiv.), Pd on carbon (5%, 42 mg, 19.9 µmol, 0.3 equiv.) and THF (30 mL) were introduced into a pressure bomb. Then hydrazine monohydrate (320 µL, 0.662 mmol, 100 equiv.) was added to the mixture before closing the bomb by a Teflon seal. The mixture was stirred at 80 °C for 48 hours. The solution was then diluted with MeOH (100 mL) before air was bubbled in the mixture at 40 °C for 24 hours. After evaporation of the solvent, the residue was purified on alumina column chromatography (DCM/MeOH 10/0 to 8/2) to afford the product as dark solid (30 mg, 29.7 µmol, 45%).

^{1}H NMR (400 MHz, CD_3OD): δ = 7.54 – 7.34 (m, 16H, ArH), 6.65 (s, 2H, CH), 6.34 (s, 2H, CH), 1.35 (s, 36H, CH_3), –2.37 (br s, 4H, ArH). Only incomplete ^{13}C NMR spectrum were recorded due to poorly resolved signals (Figure S17). **HRMS (ESI-TOF):** calcd. for $C_{64}H_{72}N_{12}^{2\bullet 2+}$ ($[M+2H]^{2+2\bullet}$) 504.2996, found 504.2997.

Synthesis of N^2,N^4,N^{14},N^{16}-tetrakis(4-(trifluoromethyl)phenyl)-azacalixphyrin (3c)

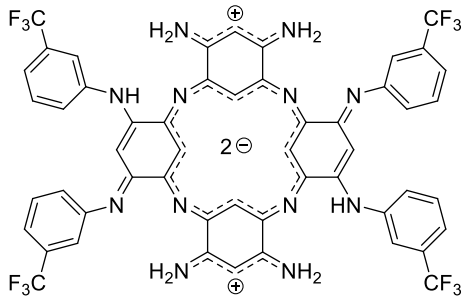

Compound **7c** (75mg, 63,05 µmol, 1 equiv), Pd on carbon (5%, 40 mg, 1.89 µmol, 0.3 equiv.) and THF (50 mL) were introduced into a pressure bomb. Then hydrazine monohydrate (250 µL, 0.635 mmol, 100 equiv.) was added to the mixture before closing the bomb with a Teflon seal. The mixture was stirred at 80 °C for 3 days. The solution was then diluted with MeOH (100 mL) before air was bubbled in the mixture at 40 °C for 2 days. After evaporation of the solvent, the residue was purified on alumina column chromatography (DCM/MeOH 10/0 to 8/2) to afford the product as dark solid (36 mg, 34 µmol, 53%).

^{1}H NMR (400 MHz, CD_3OD): δ = 7.96 – 7.31 (m, 16H, ArH), 6.86 (s, 2H, CH), 6.10 (s, 2H, CH), -1.09 (br s, 2H, ArH), –1.43 (br s, 2H, ArH). No ^{13}C NMR spectrum could be recorded due to poorly resolved signals and poor solubility (Figure S19). **HRMS (ESI-TOF):** calcd. for $C_{52}H_{35}N_{12}F_{12}^+$ ([M+H]$^+$) 1055.2911, found 1055.2910.

S-III. ^{1}H AND ^{13}C NMR SPECTRA

Compound 4c

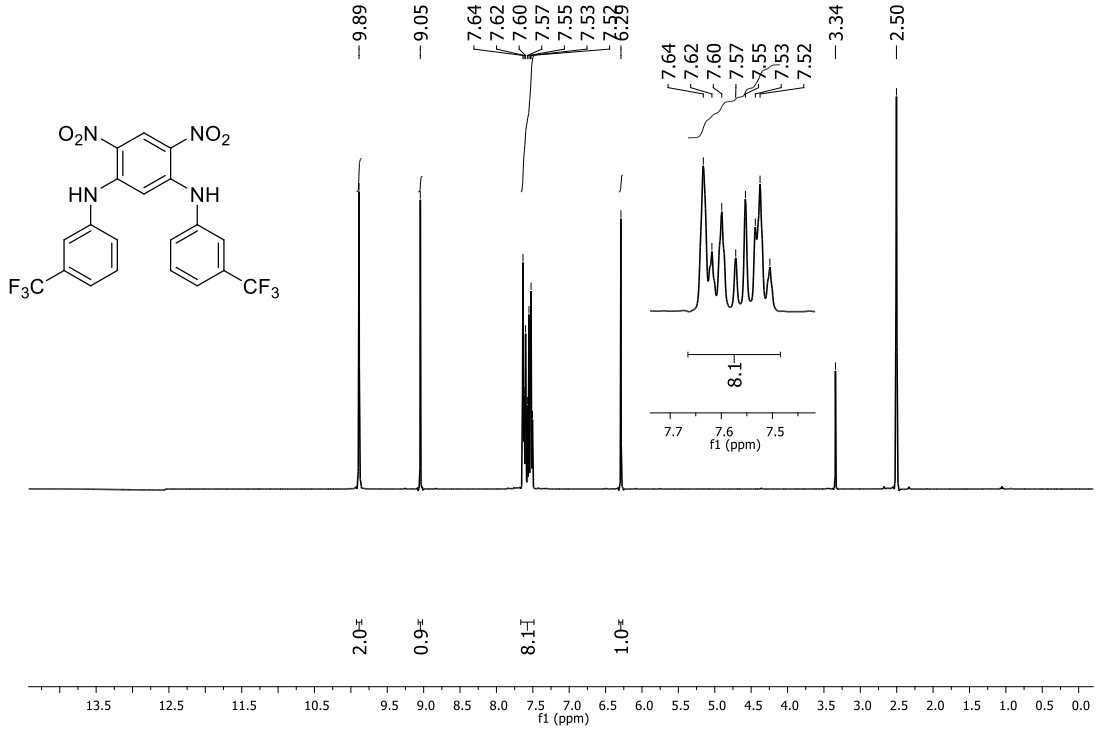

Figure S1. ^{1}H NMR (400 MHz, DMSO-*d6*) for compound **4c**.

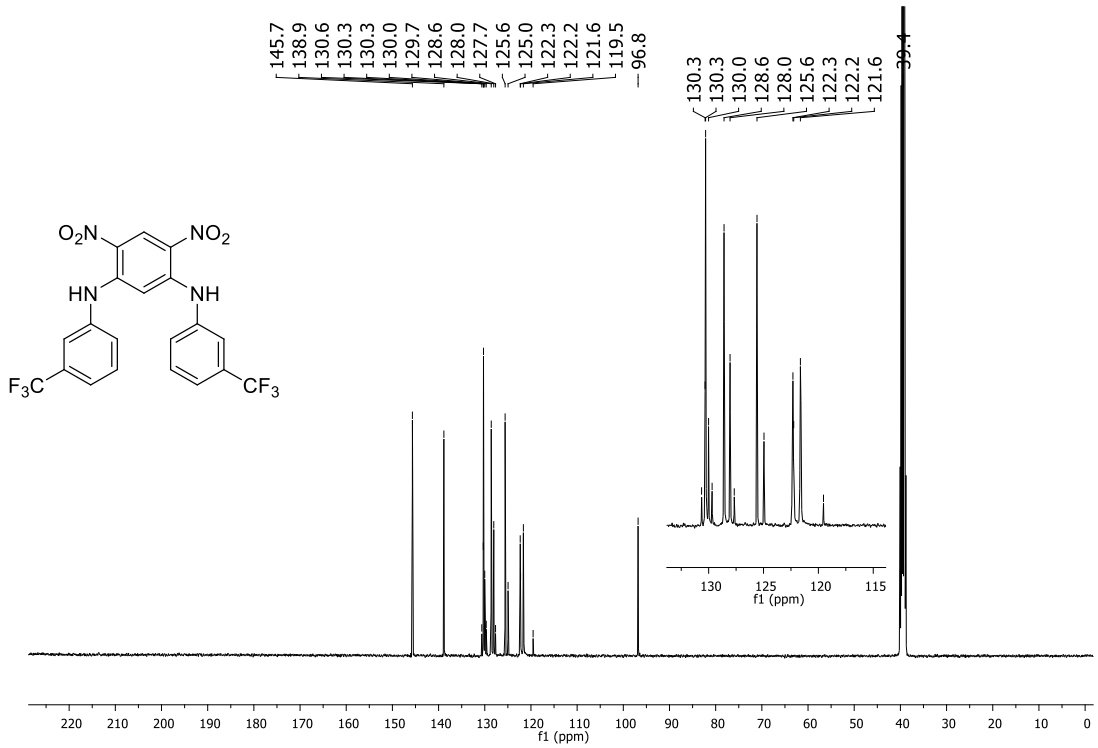

Figure S2. ^{13}C NMR (101 MHz, DMSO-*d6*) for compound **4c**.

Compound 5c

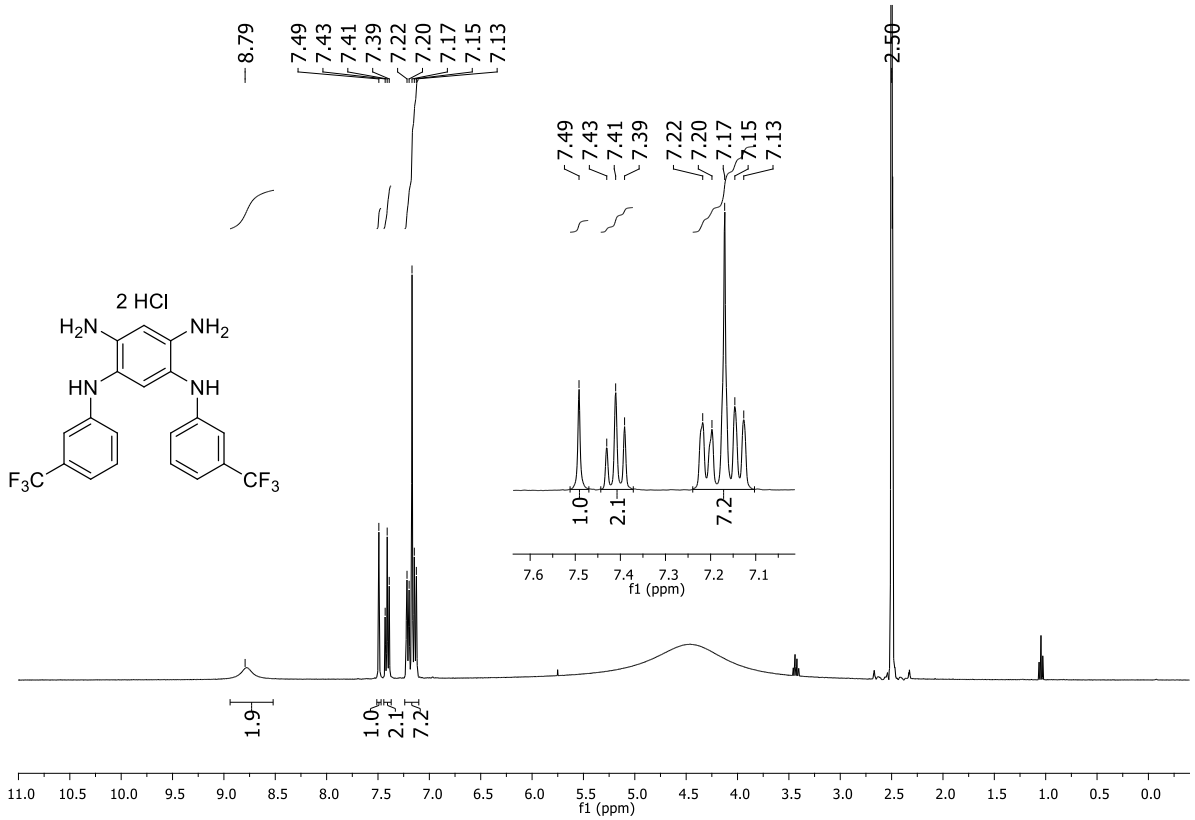

Figure S3. ^{1}H NMR (400 MHz, DMSO-*d6*) for compound **5c**.

Compound 6a

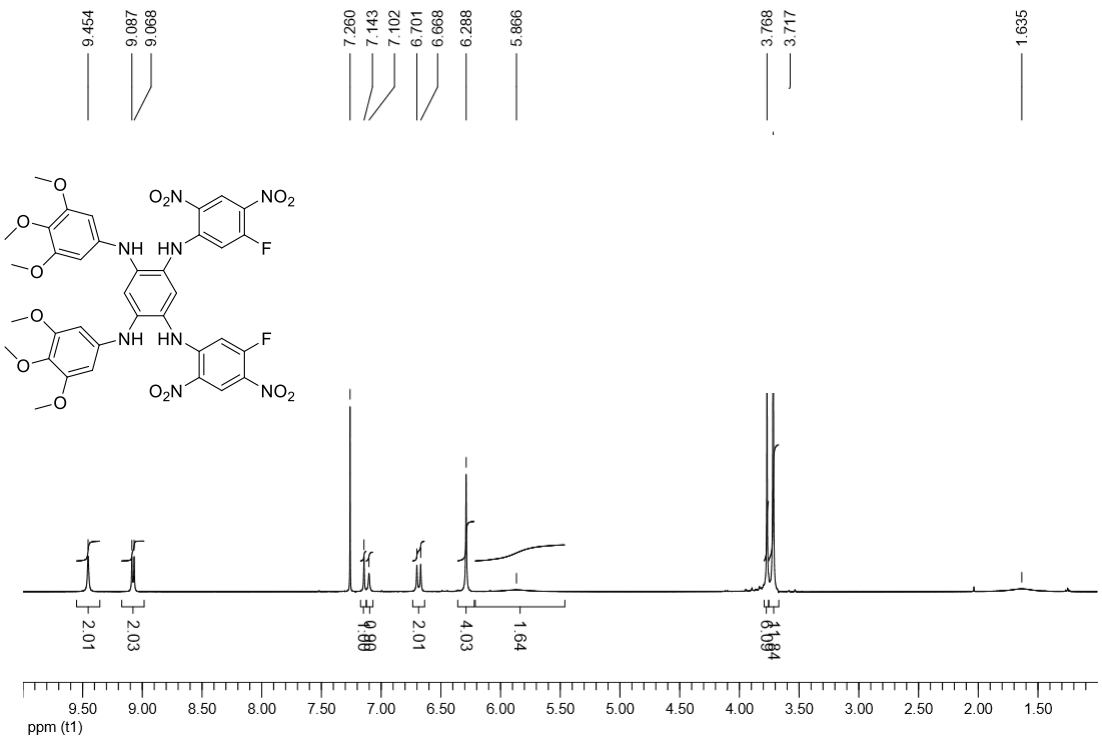

Figure S4. ^{1}H NMR (400 MHz, $CDCl_3$) for compound **6a**.

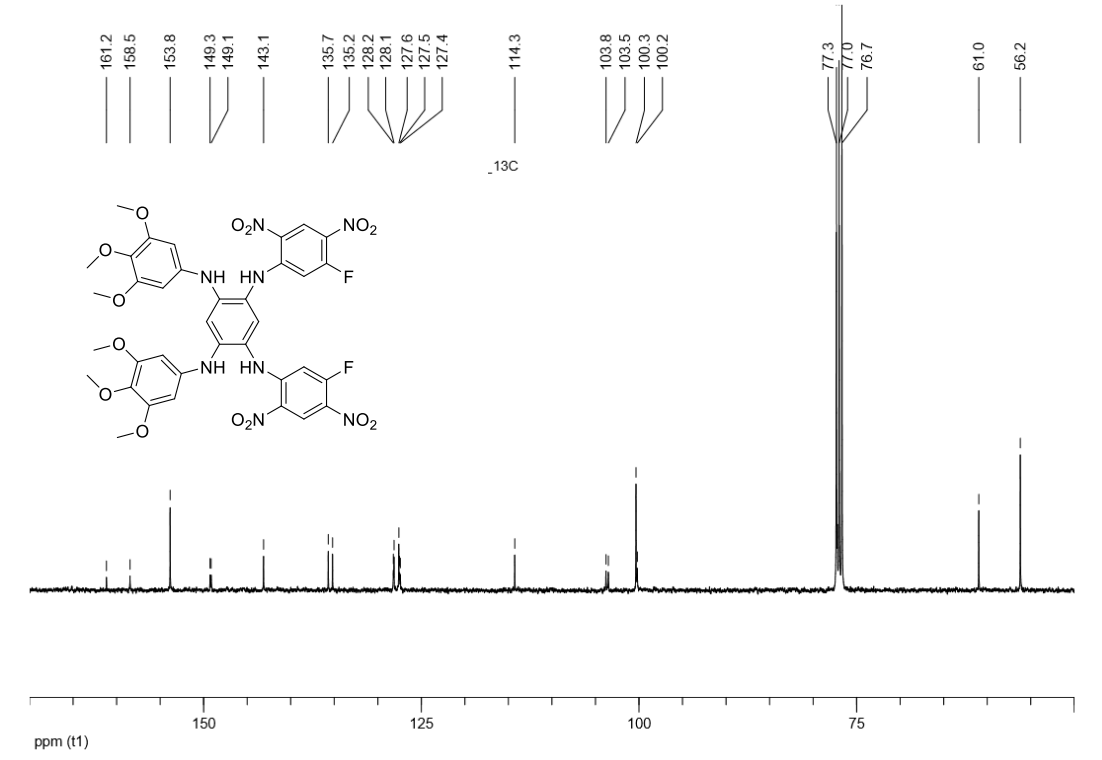

Figure S5. ^{13}C NMR (101 MHz, $CDCl_3$) for compound **6a**.

Compound 6b

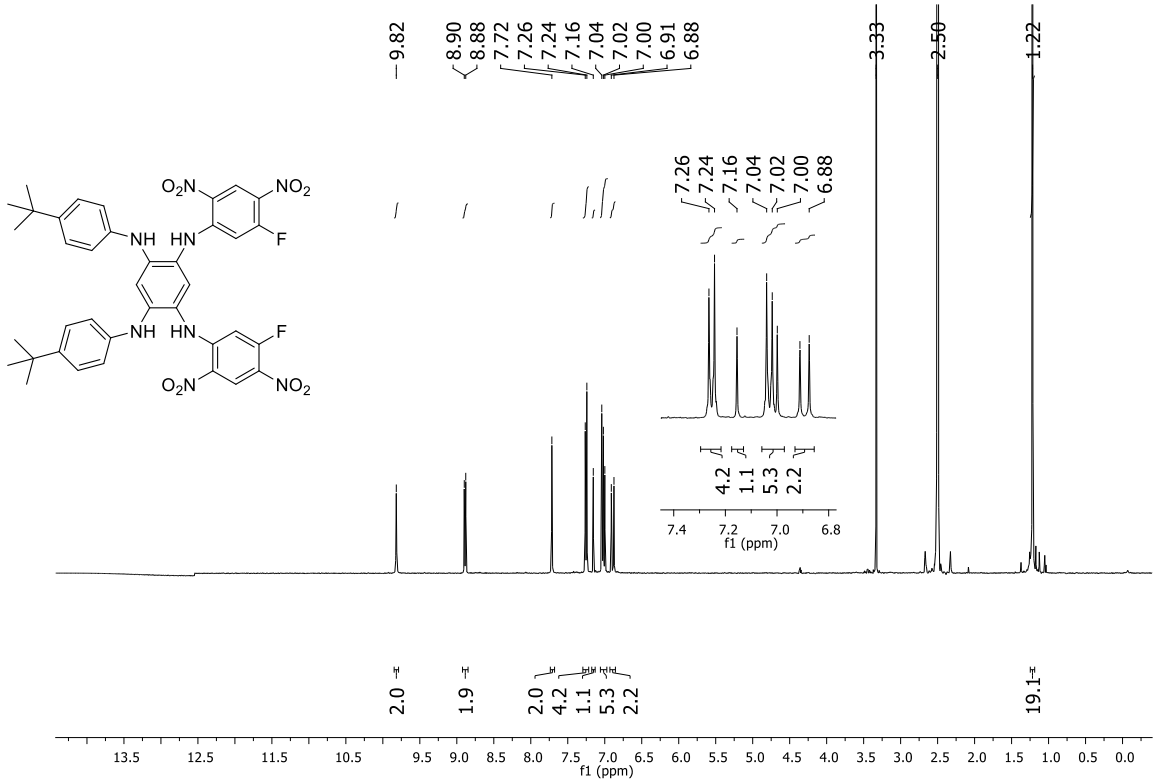

Figure S6. ^{1}H NMR (400 MHz, DMSO-*d6*) for compound **6b**.

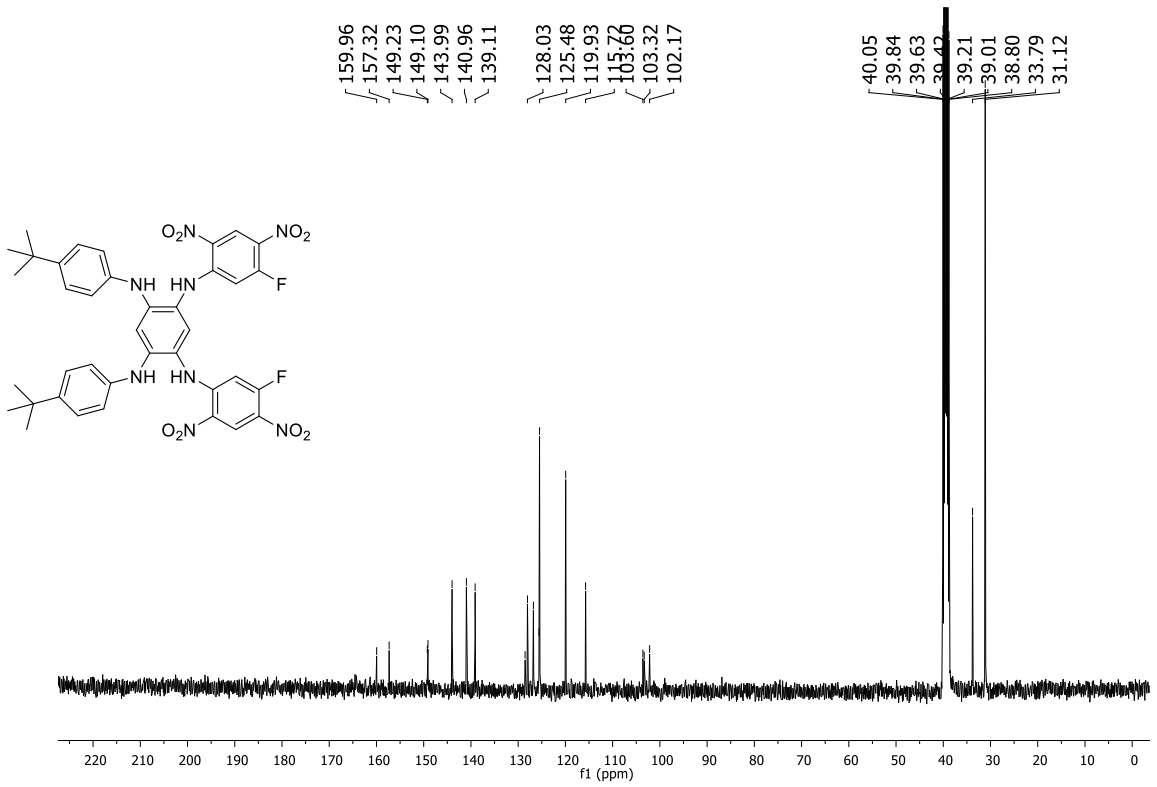

Figure S7. ^{13}C NMR (101 MHz, DMSO-*d6*) for compound **6b**.

Compound 6c

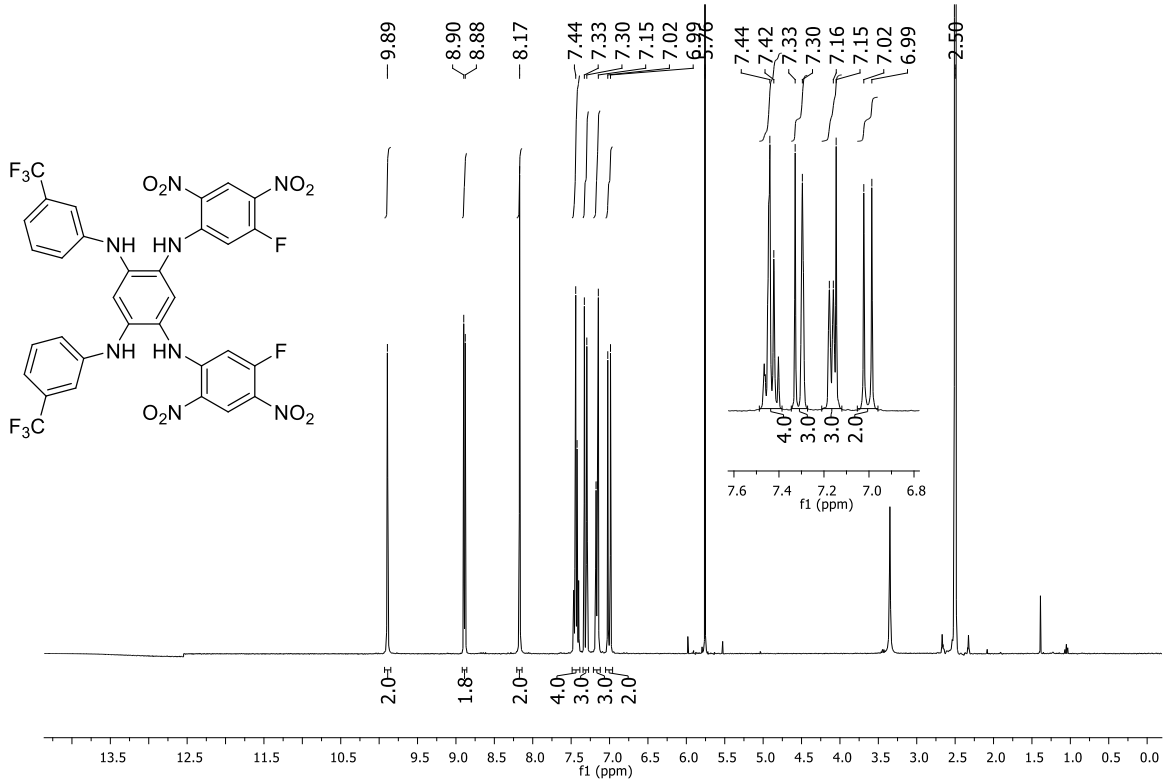

Figure S8. ^{1}H NMR (400 MHz, DMSO-*d6*) for compound **6c**.

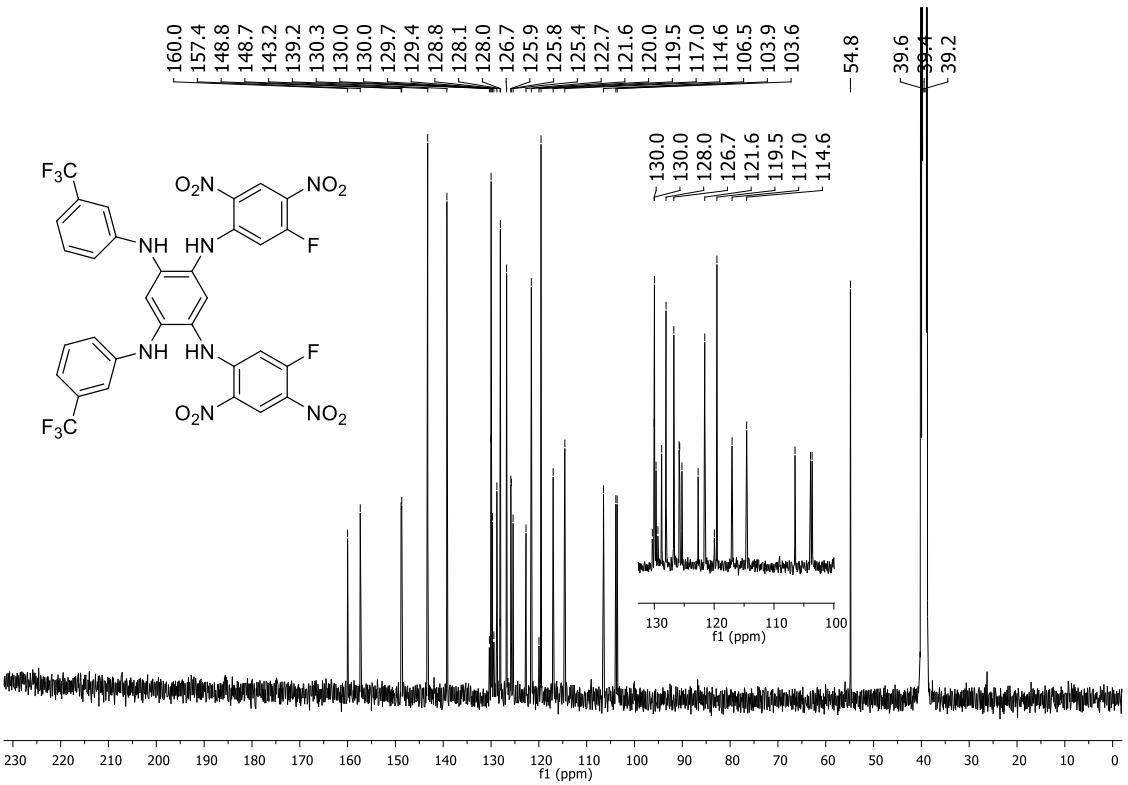

Figure S9. ^{13}C NMR (101 MHz, DMSO-*d6*) for compound **6c**.

Compound 7a

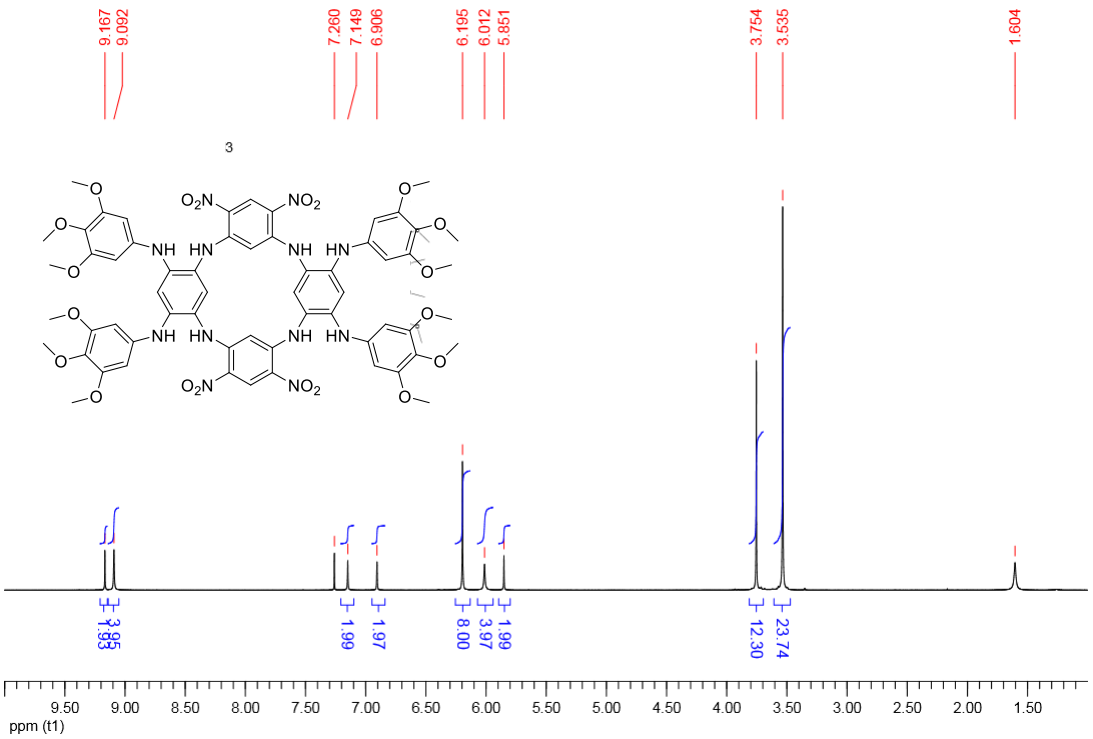

Figure S10. ^{1}H NMR (400 MHz, $CDCl_3$) for compound **7a**.

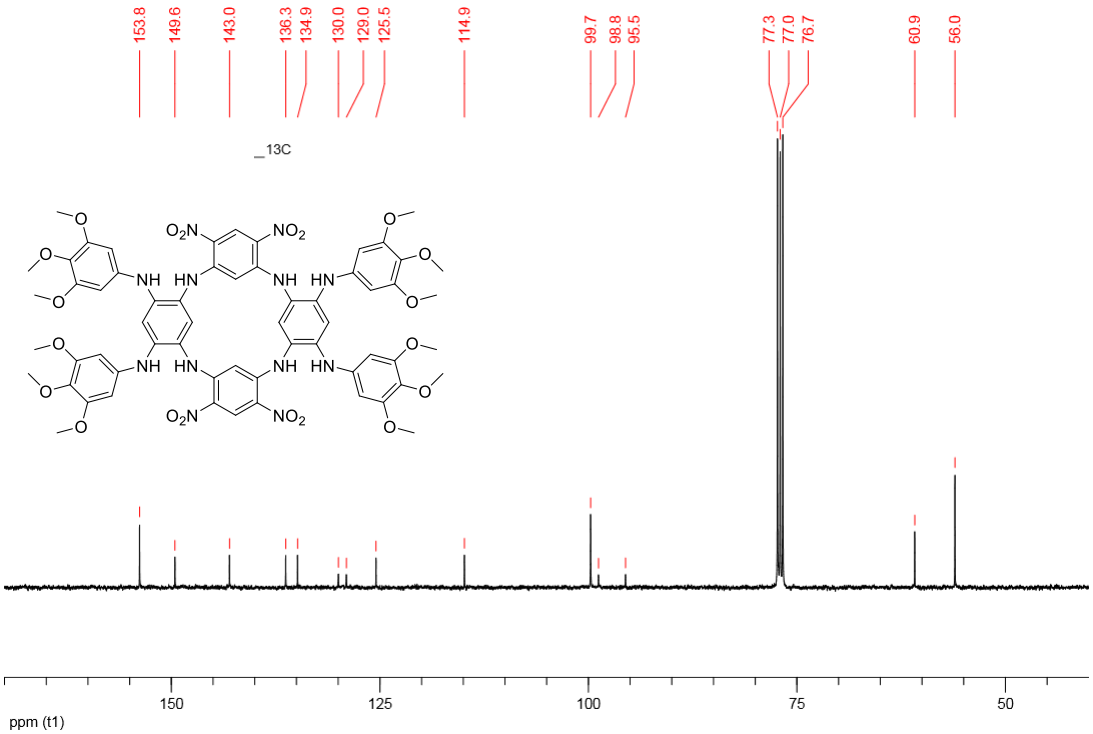

Figure S11. ^{13}C NMR (101 MHz, $CDCl_3$) for compound **7a**.

Compound 7b

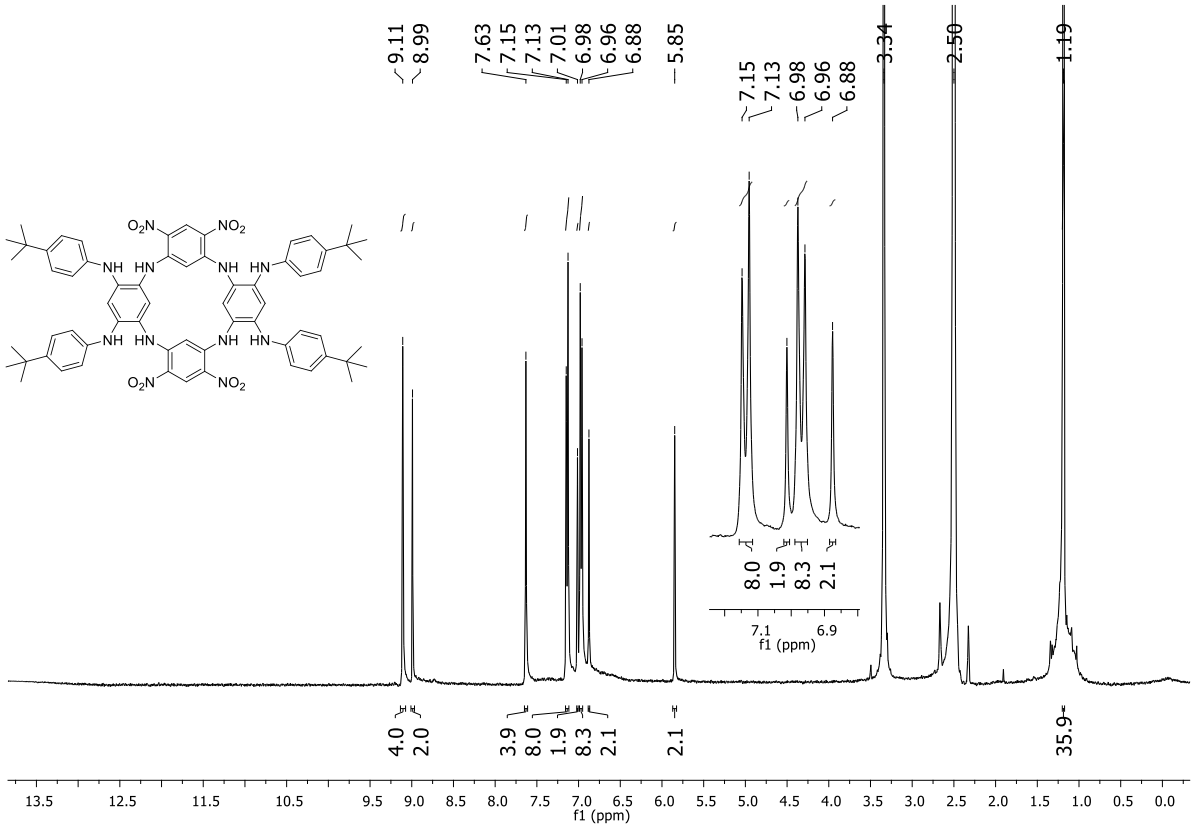

Figure S12. ^{1}H NMR (400 MHz, DMSO-*d6*) for compound **7b**.

Compound 7c

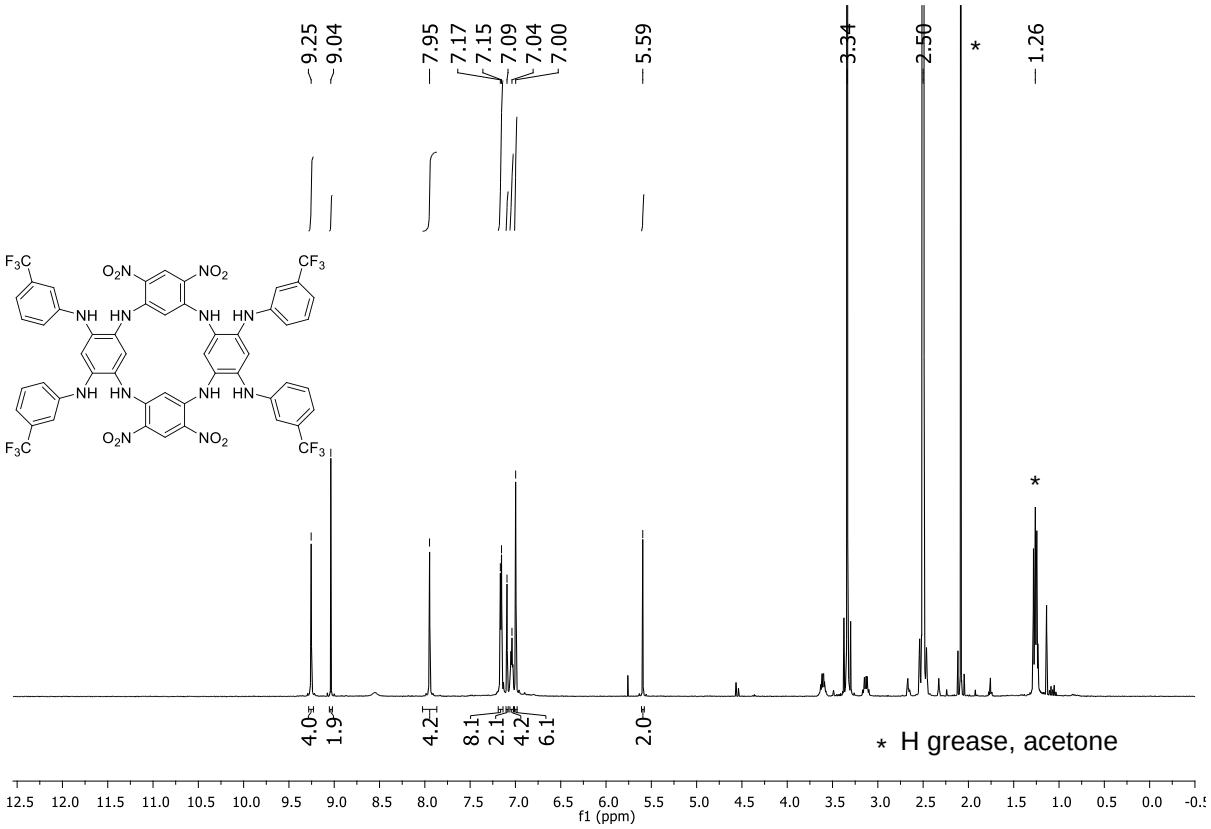

Figure S13. ^{1}H NMR (400 MHz, DMSO-*d6*) for compound **7c**.

Compound 3a

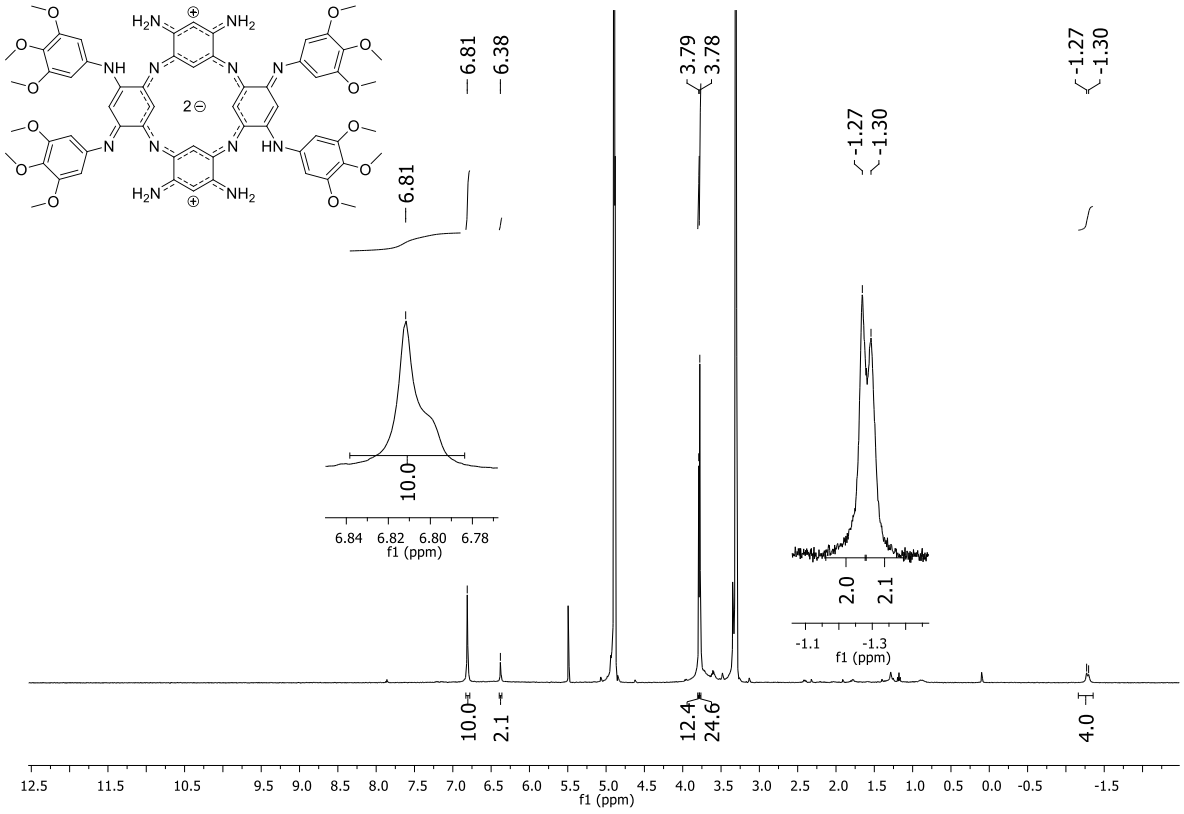

Figure S14. ^{1}H NMR (400 MHz, MeOD) for compound **3a**.

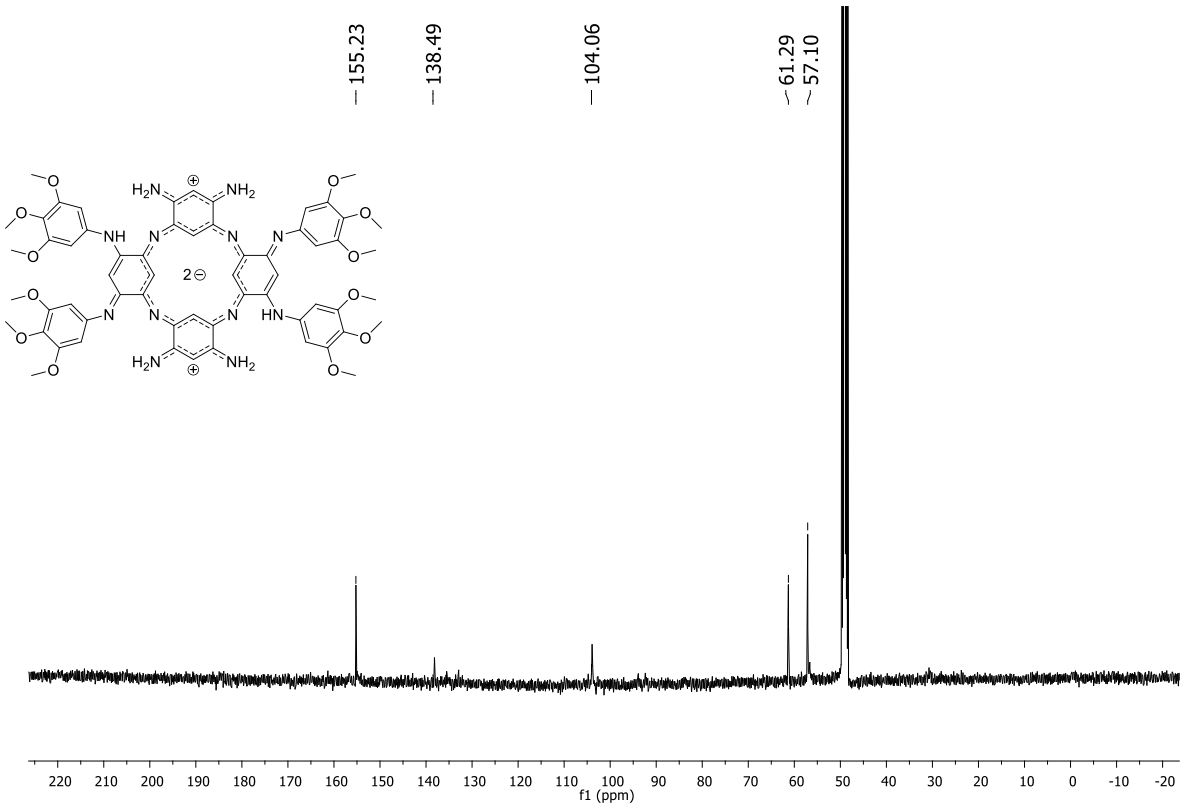

Figure S15. ^{13}C NMR (101 MHz, MeOD) for compound **3a**.

Compound 3b

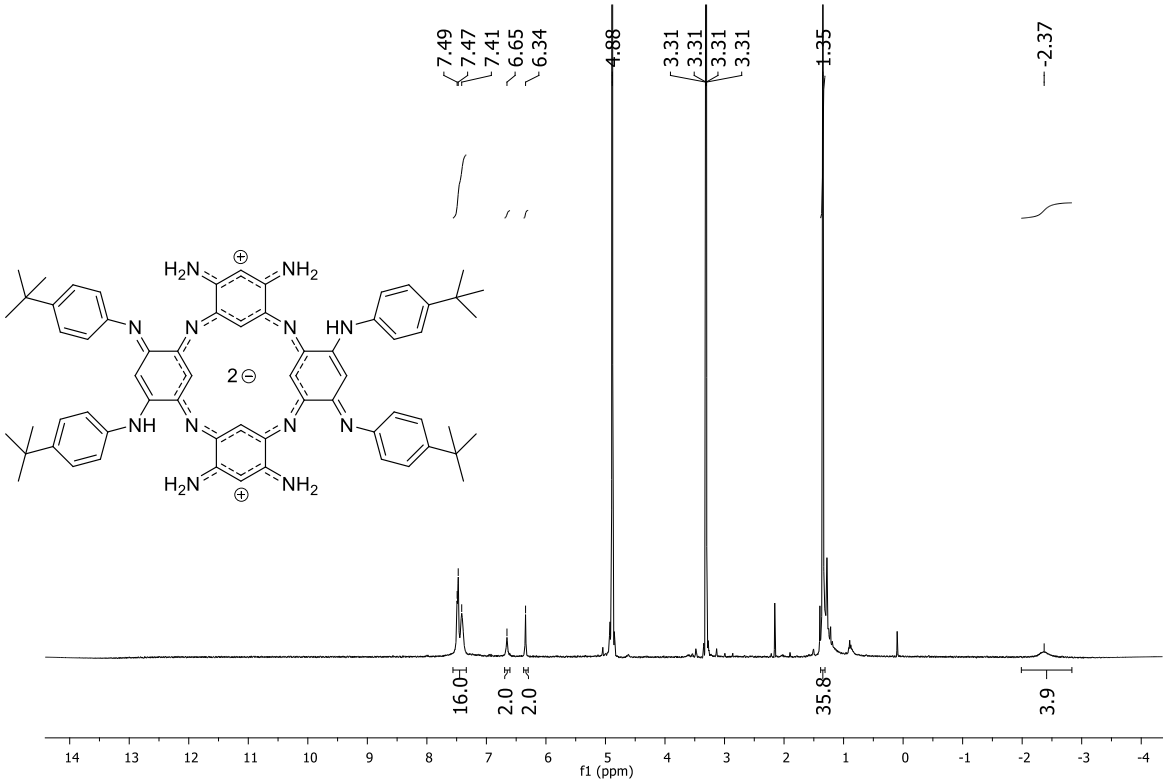

Figure S16. ^{1}H NMR (400 MHz, MeOD) for compound **3b**.

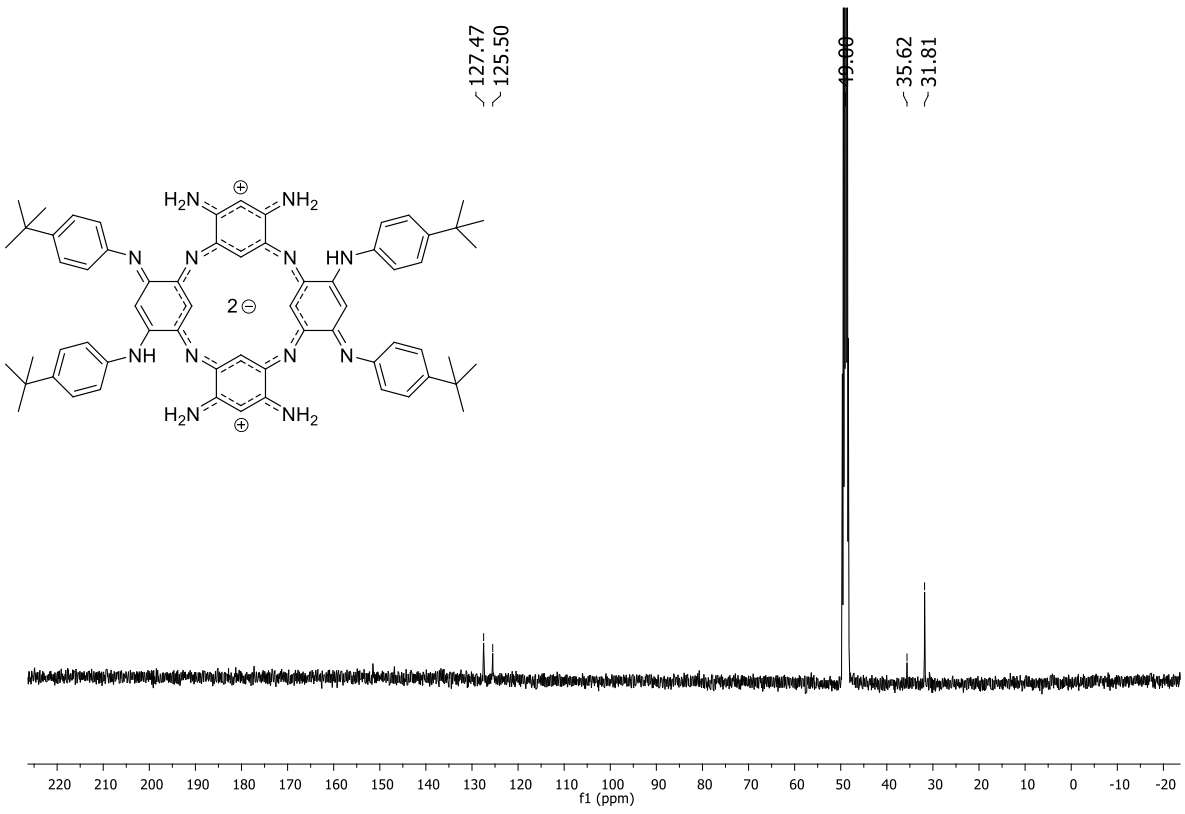

Figure S17. ^{13}C NMR (101 MHz, MeOD) for compound **3b**.

Compound 3c

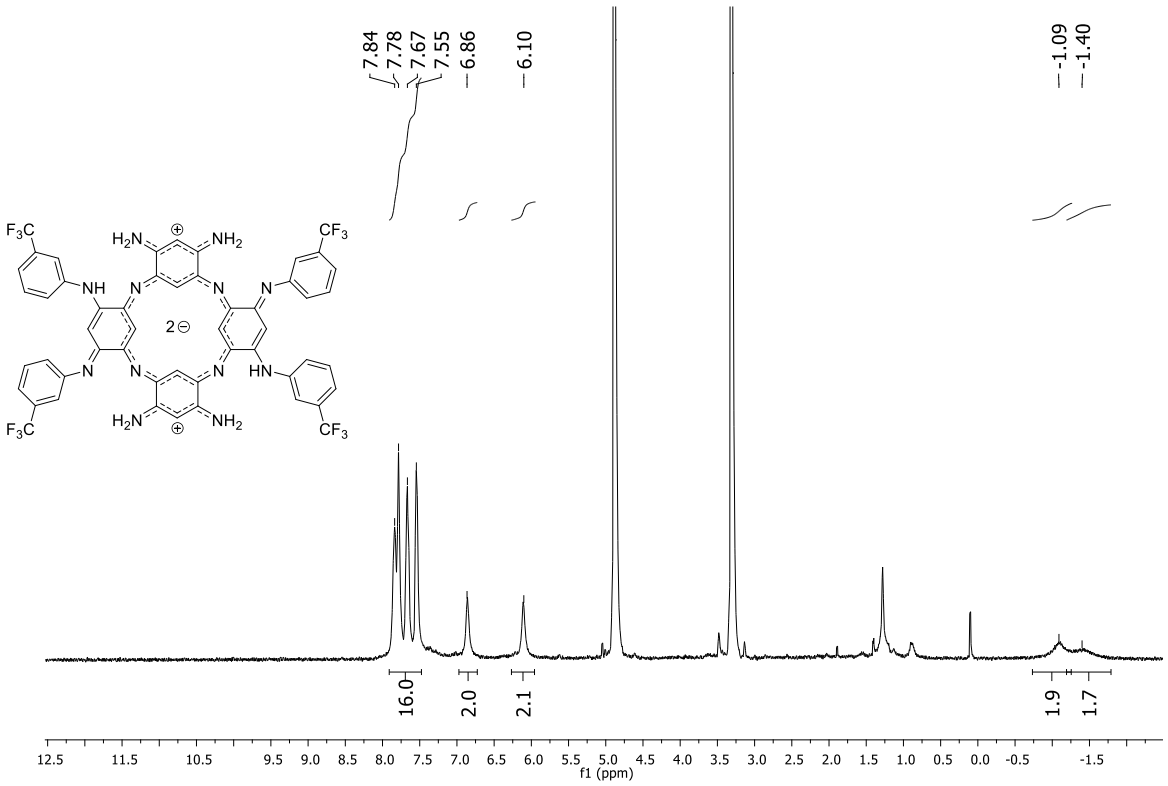

Figure S18. ^{1}H NMR (400 MHz, MeOD) for compound **3c**.

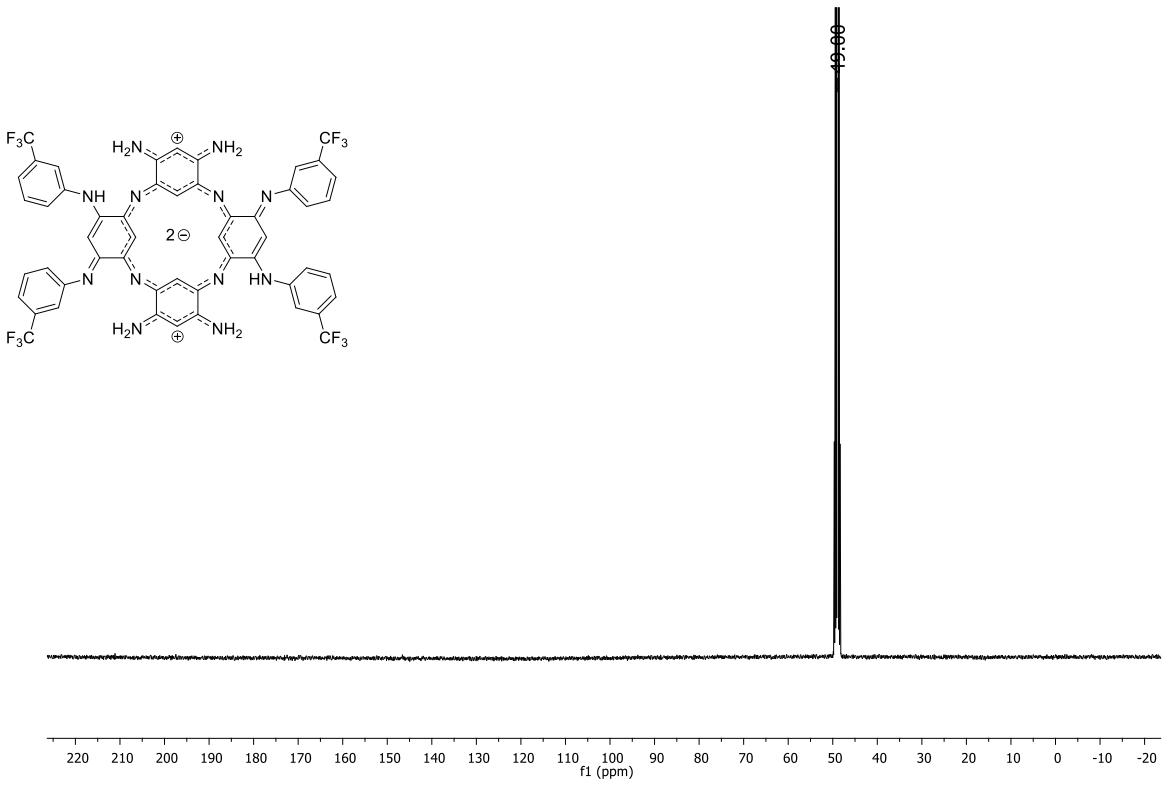

Figure S19. ^{1}H NMR (101 MHz, MeOD) for compound **3c**.

S-I. ELECTRONIC ABSORPTION AND TITRATIONS

Table S1. Optical properties of ACPs in MeOH, DMF and DMSO, without or with presence of 0.1 M trifluoroacetic acid (TFA) or 1,8-diazabicyclo[5.4.0]undec-7-ene (DBU).

Dye	MeOH			DMF			DMSO		
	Solvent only	TFA	DBU	Solvent only	TFA	DBU	Solvent only	TFA	DBU
	λ_{abs} (nm) ε ($M^{-1}.cm^{-1}$)	λ_{abs} (nm) ε ($M^{-1}.cm^{-1}$)	λ_{abs} (nm) ε ($M^{-1}.cm^{-1}$)	λ_{abs} (nm) ε ($M^{-1}.cm^{-1}$)	λ_{abs} (nm) ε ($M^{-1}.cm^{-1}$)	λ_{abs} (nm) ε ($M^{-1}.cm^{-1}$)	λ_{abs} (nm) ε ($M^{-1}.cm^{-1}$)	λ_{abs} (nm) ε ($M^{-1}.cm^{-1}$)	λ_{abs} (nm) ε ($M^{-1}.cm^{-1}$)
1	877 *5600*	886 *8000*	873 *3500*	882 *3600*	884 *7700*	891 *4000*	882 *6900*	882 *7200*	891 *3800*
2	893 *13900*	894 *14500*	895 *11300*	893 *11900*	895 *14400*	864 *5300*	896 *14200*	897 *14900*	874 *6900*
3a	938 *19900*	941 *21200*	807 *840*	851 *10800*	947 *20800*	761 *10700*	900 *8400*	944 *21500*	770 *13600*
3b	931 *21700*	936 *21600*	808 *6700*	926 *18200*	940 *21800*	759 *13200*	930 *16800*	938 *20600*	794 *11600*
3c	940 *19900*	955 *19000*	839 *9800*	816 *12000*	959 *17400*	839 *9900*	914 *16700*	964 *18300*	820 *13200*

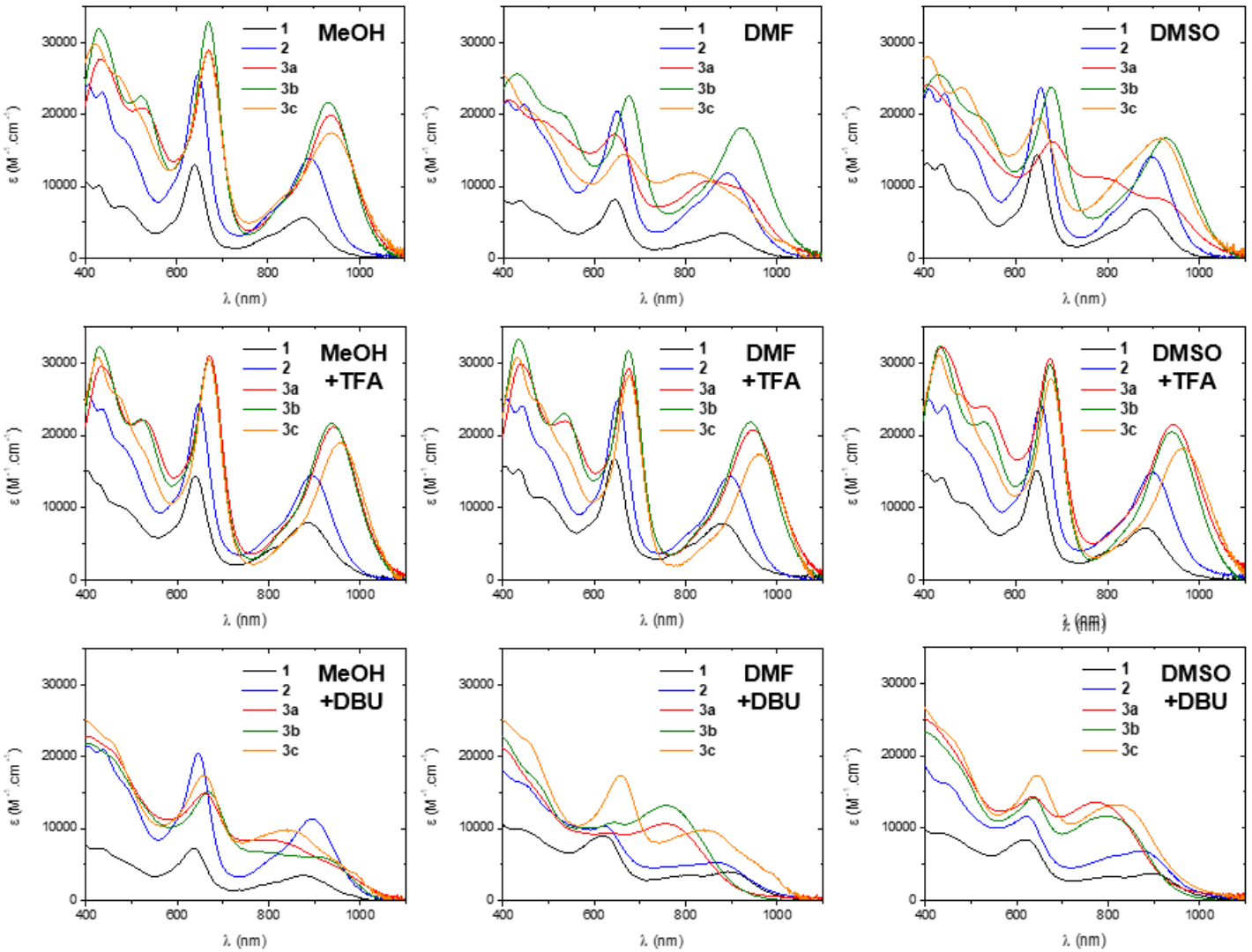

Figure S20. Electronic absorption spectra of ACPs (2.10^{-5} M) in MeOH, DMSO and DMF, without or with presence of 0.1 M trifluoroacetic acid (TFA) or 0.1 M 1,8-diazabicyclo[5.4.0]undec-7-ene (DBU).

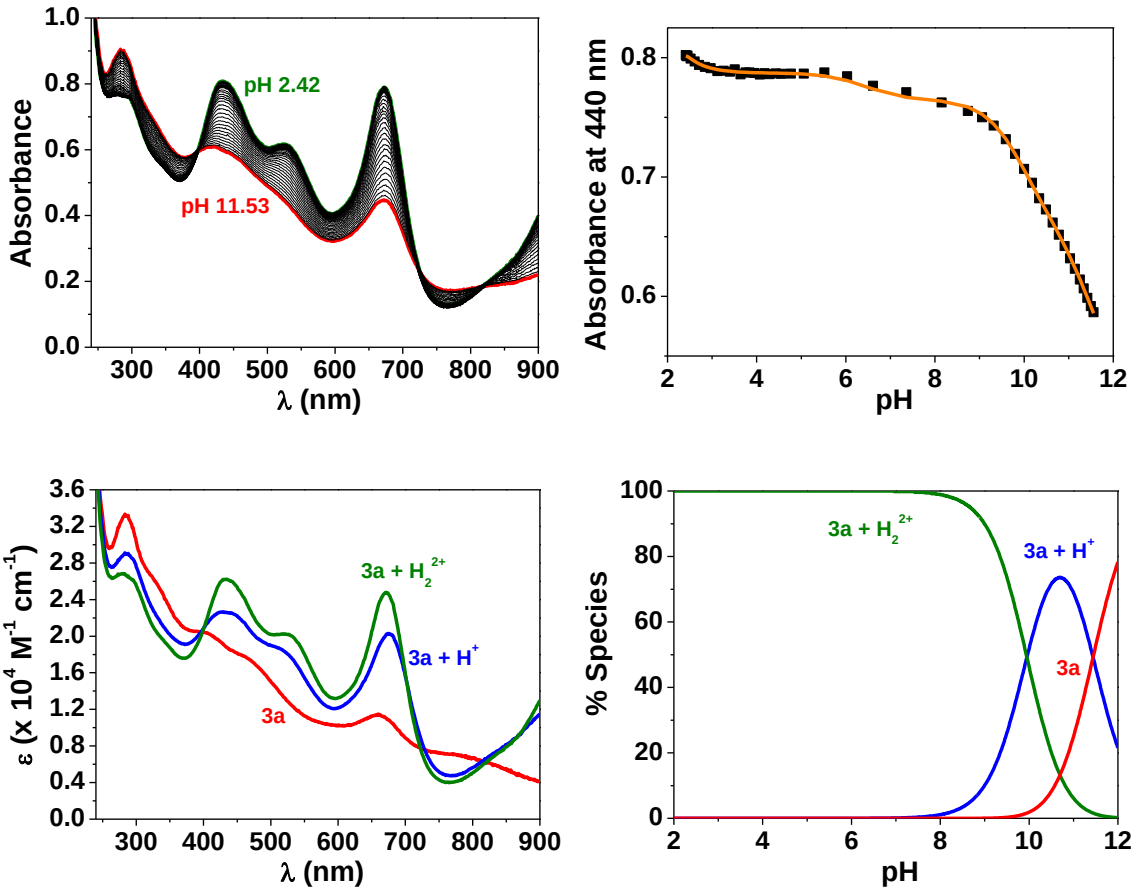

Figure S21. Absorption spectra *vs.* pH titration of **3a** (top left); variation of the absorbance at 440 nm vs. pH (top right); electronic absorption spectra of the protonated species of **3a** (bottom left); and distribution diagrams of the protonated species of **3a** as a function of pH (bottom right). Solvent: CH_3OH/H_2O (80/20 w/w); *I* = 0.1 M NBu_4ClO_4; T = 25.0 °C; [**3a**] = 2.19 x 10^{-5}M. The absorption spectra are not corrected from dilution effects. For the variation of the absorbance at 440 nm vs. pH (top right), the squares designate the experimental absorbance values recorded as a function of pH, while the orange curve describes the results of the fitting process using the Specfit program.

$\log K_{\mathbf{3a+H}} = 11.5 \pm 0.3$ (pK_{a2})

$\log K_{\mathbf{3a+H2}} = 9.9 \pm 0.3$ (pK_{a1})

To justify the use of a model containing two protonated species of **3a**, the figures provided below show the results of different models assuming no protonation, a monoprotonated species, a diprotonated species and a mixture of mono- and diprotonated species. Figure S22 first shows a comparison between the experimental data (black circles) and the theoretical curve (orange line) for a model that does not involve any deprotonation. One can clearly see that absorption variations under acidic pH (2 to 6) and basic pH (pH > 11) originate from dilution effects induced by the addition of base required to adjust the pH from ~2 to ~12.

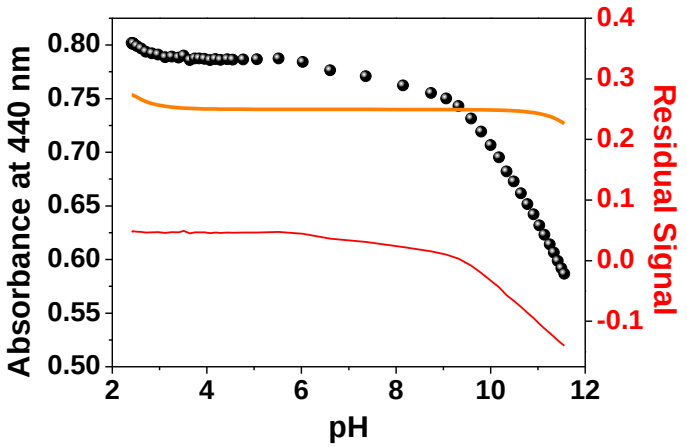

Figure S22. 1st Model: No deprotonation (**3a** alone) – (left axis) Variation of the absorbance at 440 nm vs. pH (the black circles designate the experimental absorbance values recorded as a function of pH, while the orange curve describes the results of the fitting process using the Specfit program and the corresponding model). (right axis) residual signal (red curve) that designates the difference between the experimental and the theoretical data. Solvent: CH_3OH/H_2O (80/20 w/w); *I* = 0.1 M NBu_4ClO_4; T = 25.0 °C; [**3a**] = 2.19 x 10^{-5}M. The absorption spectra are not corrected from dilution effects.

Figure S23 then depicts a model with only one protonation constant (i.e., only one protonated species, [**3a**+H]$^+$ in addition to **3a**). One can also clearly see that the theoretical curve does also not account for the variation of absorbance at 440 nm.

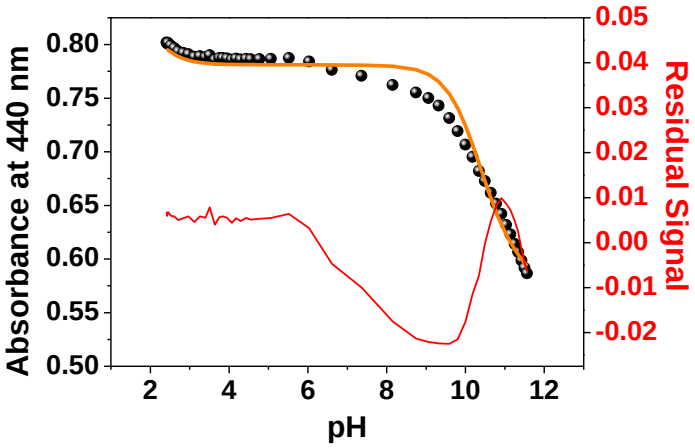

Figure S23. 2nd Model: One protonated species ([**3a**+H]$^+$ in addition to **3a**) – (left axis) Variation of the absorbance at 440 nm vs. pH (the black circles designate the experimental absorbance values recorded as a function of pH, while the orange curve describes the results of the fitting process using the Specfit program). (right axis) residual signal (red curve) that shows the difference between the experimental and the theoretical data. Solvent: CH_3OH/H_2O (80/20 w/w); *I* = 0.1 M NBu_4ClO_4; T = 25.0 °C; [**3a**] = 2.19 x 10^{-5}M. The absorption spectra are not corrected from dilution effects.

With respect to a model containing a diprotonated species ([**3a**+2H]$^{2+}$ in addition to **3a**) that is associated to a global protonation constant, Figure S24 demonstrates that the theoretical curve does also not account for the variation of absorbance at 440 nm.

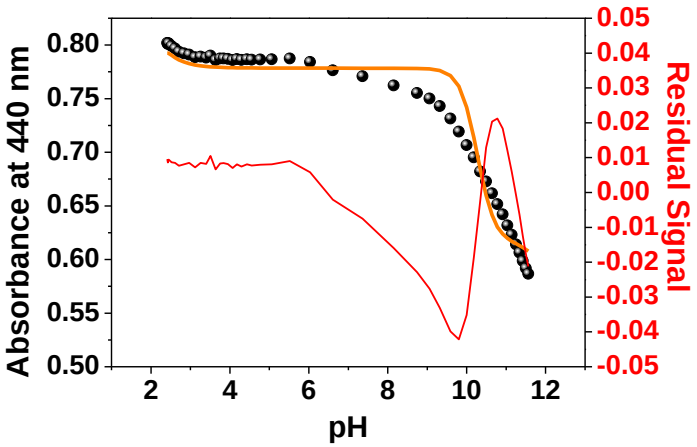

Figure S24. 3rd Model: two protonated species ([**3a**+H]$^{+}$ and [**3a**+2H]$^{2+}$ in addition to **3a**) with a global protonation constant –(left axis) Variation of the absorbance at 440 nm vs. pH (the black circles designate the experimental absorbance values recorded as a function of pH, while the orange curve describes the results of the fitting process using the Specfit program). (right axis) residual signal (red curve) that shows the difference between the experimental and the theoretical data. Solvent: CH_3OH/H_2O (80/20 w/w); *I* = 0.1 M NBu_4ClO_4; T = 25.0 °C; [**3a**] = 2.19 x 10^{-5}M. The absorption spectra are not corrected from dilution effects.

Lastly, Figure S25 depicts the results assuming two successive protonated species ([**3a**+H]$^{+}$ and [**3a**+2H]$^{2+}$ in addition to **3a**) related to two protonation constants. Two pK_a (log K_{3a+H} = 11.5 ± 0.3 (pK_{a2}) and log K_{3a+H2} = 9.9 ± 0.3 (pK_{a1})) were determined and correspond to average values resulting from duplicate experiments.

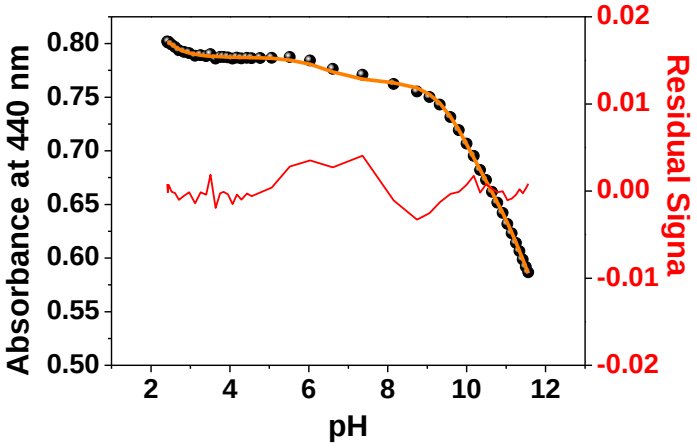

Figure S25. 4th Model: two protonated species ([**3a**+H]$^{+}$ and [**3a**+2H]$^{2+}$ in addition to **3a**) with two successive protonation constant – (left axis) Variation of the absorbance at 440 nm vs. pH (the black circles designate the experimental absorbance values recorded as a function of pH, while the orange curve describes the results of the fitting process using the Specfit program). (right axis) residual signal (red curve) that shows the difference between the experimental and the theoretical data. Solvent: CH_3OH/H_2O (80/20 w/w); *I* = 0.1 M NBu_4ClO_4; T = 25.0 °C; [**3a**] = 2.19 x 10^{-5}M. The absorption spectra are not corrected from dilution effects.

S-II. PHOTOACOUSTIC

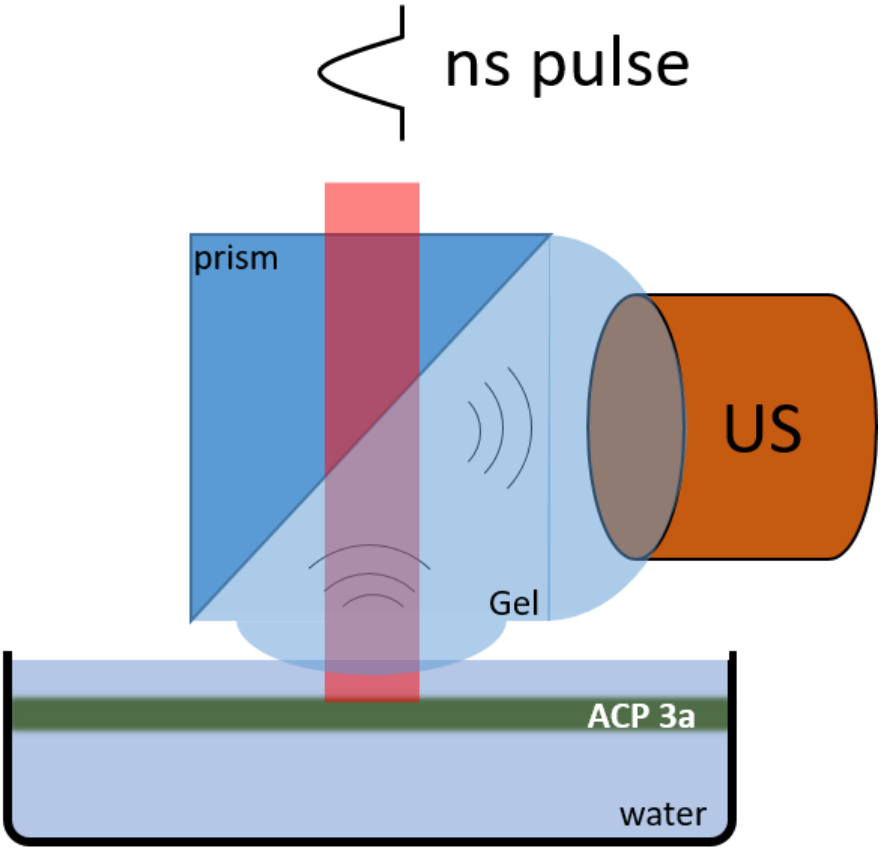

Figure S26. Representation of the experimental photoacoustic setup (ns = nanosecond, US = ultrasound transducer, ACP = azacalixphyrin).

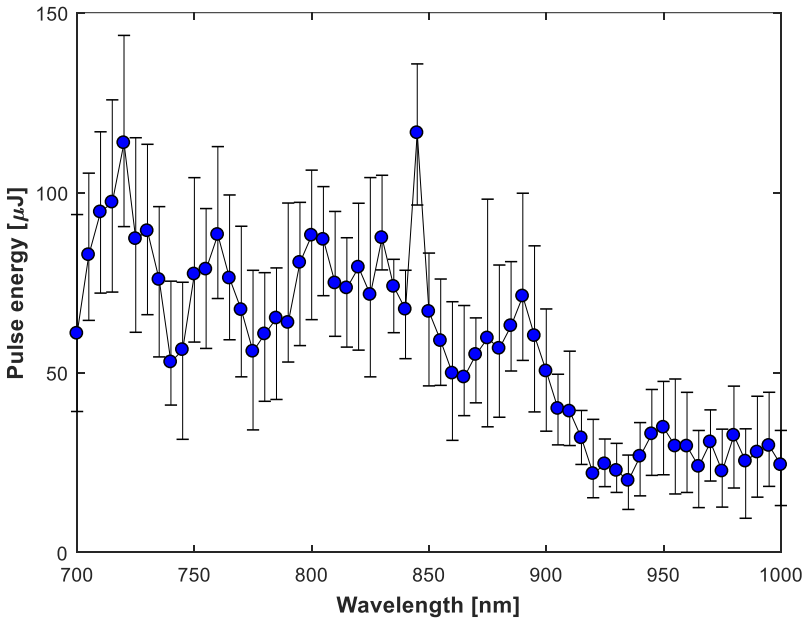

Figure S27. The mean value of the intensity measured with a photodiode at the end of the optical path is used to correct for the laser wavelength spectrum.

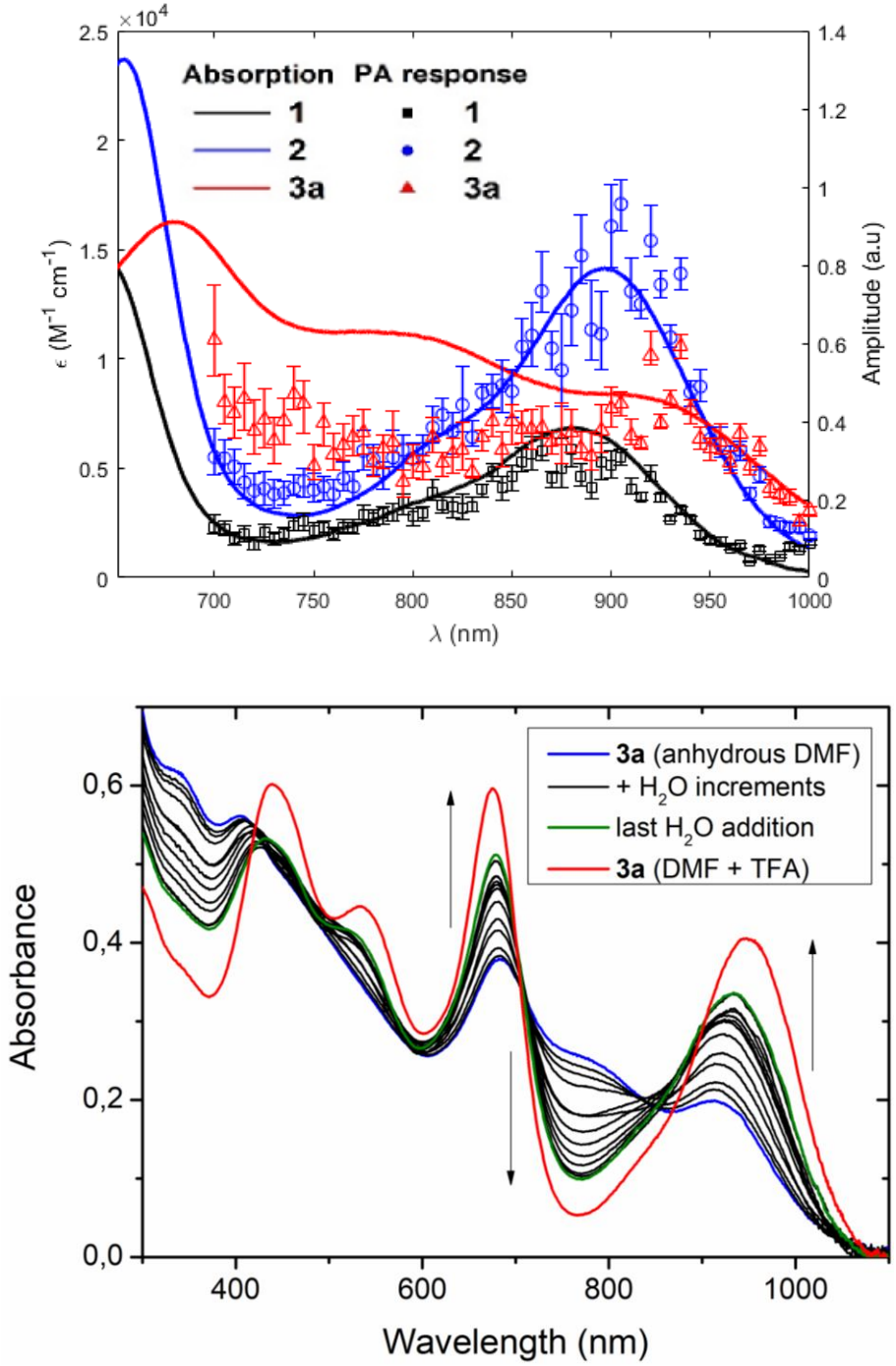

Figure S28. Top: Vis-NIR electronic absorption spectra **1** (–––), **2** (——), **3a** (——) compared to photoacoustic amplitude measurements of ACPs **1** (■), **2** (●), **3a** (▲) in DMSO (*ca*. 100 µM). Fluctuations observed *ca*. 900-950 nm for compound **3a** is presumably due to the presence of **3a+H⁺** and/or **3a+2H⁺** species in the DMSO solution. Bottom: Evolution of the absorption spectrum of **3a** in DMF upon addition of water and finally one drop of TFA. The data are uncorrected from dilution.

Apart from laser fluctuation reasons, we have figured out why the PA amplitude measured within the NIR range for molecule **3a** in DMSO shows some fluctuations. The general profile of PA amplitude between 900 and 950 nm differs from the previously recorded absorption in DMSO because of the presence of water traces within the solution during the OptiCell experiment. In fact when the DMSO presents traces of water, the transition *ca*. 900 nm can slightly increase due to a partial evolution of

3a towards the **3a+H**$^{+}$ and/or **3a+2H**$^{+}$ species (see Figure S20, DMSO *vs* DMSO+TFA). In DMSO the access to the pure neutral species is indeed extremely difficult owing to the presence of proton sources. To support this behavior, we studied the effect of water within a solution of **3a** in anhydrous DMF (easier to obtain than DMSO). As expected, in anhydrous DMF, the absorption profile is closed to the one reported in DMSO solution. Upon small increments of water, the 950 nm slightly increases, as a result of a protonation of **3a** (Figure S28, bottom). The profile of the spectra obtained in wet DMF solutions matches then well with the PA amplitude enhancement at 950 nm measured for **3a** in DMSO (Figure S28, top).

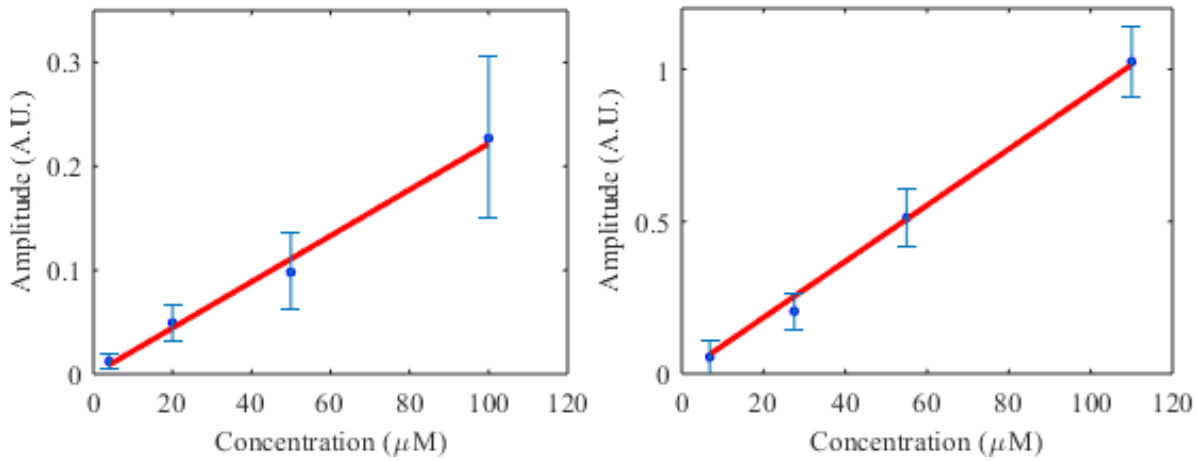

Figure S29. Maximum PA amplitude versus concentration for ACP **2** in DMSO at 900nm (left) and ACP **3a** in methanol at 938 nm (right). The absorption of solvent was corrected by substation of the offset value (intrinsic absorption of the solvent) from the raw measurements at the measured wavelength. The results were fitted to a linear function. The error bars were added based on the contribution of two phenomena: The percentage error due to laser fluctuations and the SNR detectability.

S-III. THEORETICAL MODELLING

Methods. All calculations have been made with Gaussian16,[8] using default procedures and algorithms except when noted below. We have used the PBE0[9] hybrid functional for all our calculations, and applied tighten thresholds for the energy (at least 10^{-9} au) and geometry convergences (so-called *tight* threshold in Gaussian), as well as used an improved DFT integration grid (*ultrafine* grid). For all compounds, we have optimized the ground-state geometry with the 6-31G(d) atomic basis set and subsequently verified the absence of imaginary frequencies by computing analytically the Hessian at the same level of theory. The excited-state calculations were performed with TD-DFT considering 15 states determined with the same functional and the 6-31+G(d) atomic basis set. The solvent effects were modeled through the well-known Polarizable Continuum Model (PCM),[10] using the linear-response *non-equilibrium* model for the excited-state calculations.

Results. First, we have modelled the ACP in their fully protonated forms (**X•2H$^+$**), i.e., in which all external groups are amine, as these structures do exist under a single tautomeric form.[7] For **1•2H$^+$,** theory predicts that the NIR absorption takes place at 784 nm (*f*=0.123) which is blueshifted compared to the experimental value of 882 nm (see Table S1), a fact related to the use of the vertical TD-DFT approximation (i.e., the neglect of vibronic effects). This corresponds to a deviation of 0.18 eV, typical of vertical TD-DFT for organic dyes. As expected, the NIR band of **1•2H$^+$** involves two degenerated electronic states (f=0.0615 each) and the four frontier MOs (Figure S30), that are highly-delocalized π orbitals. The addition of long alkyl chains leading to **2•2H$^+$** induce a degeneracy lifting (D_{2d} to C_{2v}), but the two first electronic states are still nearly degenerated in **2•2H$^+$** (S_1: 787.3 nm, *f*=0.131; S_2: 787.0 nm, *f*=0.072). Therefore, compared to **1•2H$^+$**, theory predicts a small bathochromic shift and a significant hyperchromic effect with a TD-DFT vertical absorption at 787 nm (*f*=0.202), both trends are totally consistent with experiment (Table S1) as well as with a previous investigation.[7] The nature of the involved MOs in this band is not significantly changed compared to **1•2H$^+$**. With substituted phenyl rings, the symmetry lowers again (to C_2) and the near-degeneracy of the two lowest excited states is more clearly lifted. In addition, and consistently with experiment, TD-DFT provides significant bathochromic and hyperchromic displacements for all three ACPs: **3a•2H$^+$** (S_1: 857.8 nm, *f*=0.388; S_2: 835.1 nm, *f*=0.081), **3b•2H$^+$** (S_1: 851.0 nm, *f*=0.353; S_2: 831.8 nm, *f*=0.094), and **3c•2H$^+$** (S_1: 852.0 nm, *f*=0.353; S_2: 835.5 nm, *f*=0.043). It remains that the same four frontier orbitals are involved in these two excited states. Illustratively, they are displayed in Figure S31 for the **3b•2H$^+$**. Globally, the shapes of the MOs are unchanged compared to the non-substituted case but there are now small contributions of the phenyl rings in the HOMO and LUMO, explaining the redshifts (compare Figures S30 and S31).

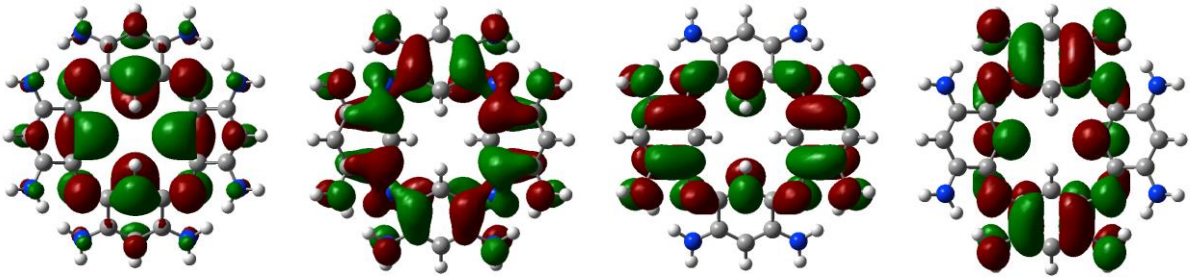

(-6.01 eV) **HOMO-1** | (-5.89 eV) **HOMO** | (-3.59 eV) **LUMO** | (-3.59 eV) **LUMO+1**

Figure S30. Representation of the four frontier MOs of **1•2H$^+$**.

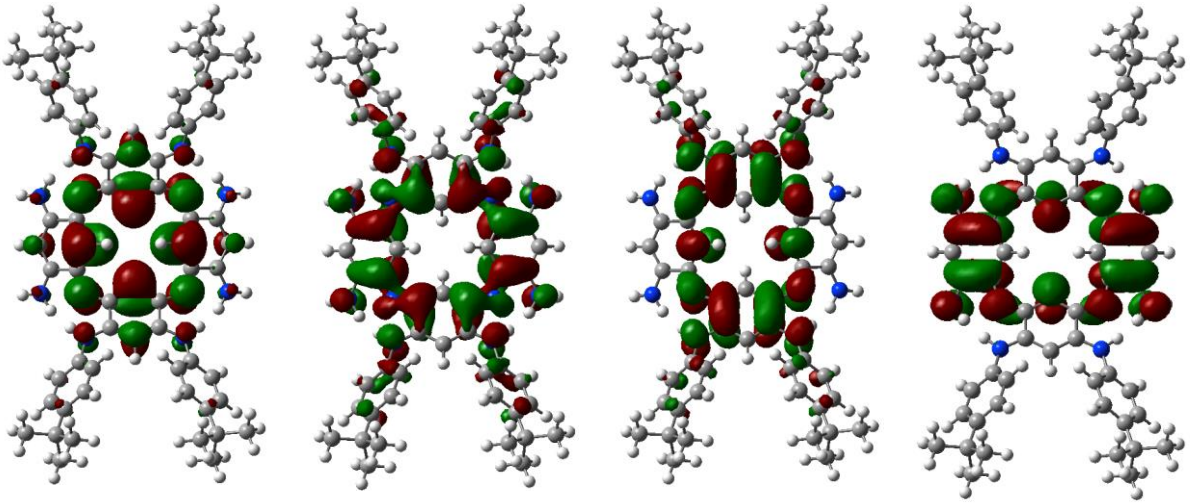

(-6.00 eV) **HOMO-1** | (-5.75 eV) **HOMO** | (-3.70 eV) **LUMO** | (-3.62 eV) **LUMO+1**

Figure S31. Representation of the four frontier MOs of **3b•2H$^+$**.

Next, for **3a**, we have modelled the properties of a series of forms presenting different protonation states (**3a•3H$^+$**; **3a•2H$^+$**; **3a•H$^+$; 3a** and **3a** - **2H$^+$**). At the exception of the **3a•3H$^+$** and **3a•2H$^+$** forms, several plausible tautomers exist and we have considered all of them following the same procedure as in ref. 7. For the sake of compactness, we however discuss only the properties of the most stable conformers of each protonation states. As stated above, the fully protonated forms, **3a•2H$^+$**, shows its lowest vertical transition at 857.8 nm (*f*=0.388) and 835.1 nm (*f*=0.081). Protonation of one of the bridging nitrogen atom (**3a•3H$^+$**) yields red- and hyperchromic shifts with transitions at 888.7 nm (*f*=0.554) and 850.5 nm (*f*=0.055). In contrast, for the systems with seven external NX_2 (X=R or H) and one external NX (X=R or H), i.e., for **3a•H$^+$**, we found peak positions almost unchanged compared to the **3a•2H$^+$** form: 854.3 nm (*f*=0.125) and 825.6 nm (*f*=0.233). However, the significant reorganization of the relative oscillator strengths seem to suggest the possibility of a broader absorption. The corresponding neutral structure (**3a**, the most stable tautomer is "2-7", see ref. 7 for details regarding the notation) again displays absorption in a very similar spectral region, but the intensity decreases, i.e., 850.8 nm (*f*=0.233) and 804.5 nm (*f*=0.007). On the reverse for the doubly

deprotonated structure (**3a** - **2H$^+$**) the changes predicted by theory are a strong hyperchromic effect accompanied by a small redshift with the two first stated at 881.2 nm (f=0.591) and 785.1 nm (f=0.179*)*. Therefore, although it is not possible to rule out the presence of both **3a•2H$^+$** and **3a•3H$^+$** in the DMSO+TFA spectra of Figure S20, the measured spectrum in DMSO+DBU that is both blueshifted and much more broad cannot correspond to the doubly deprotonated structure as this would yield a qualitative disagreement with theory. The MOs of three forms of **3a** are displayed below, in Figure S32. As can be seen the shape of the MOs are rather similar in all cases, i.e., the protonation state tunes the transition energies without strongly modifying the topology of the involved orbitals.

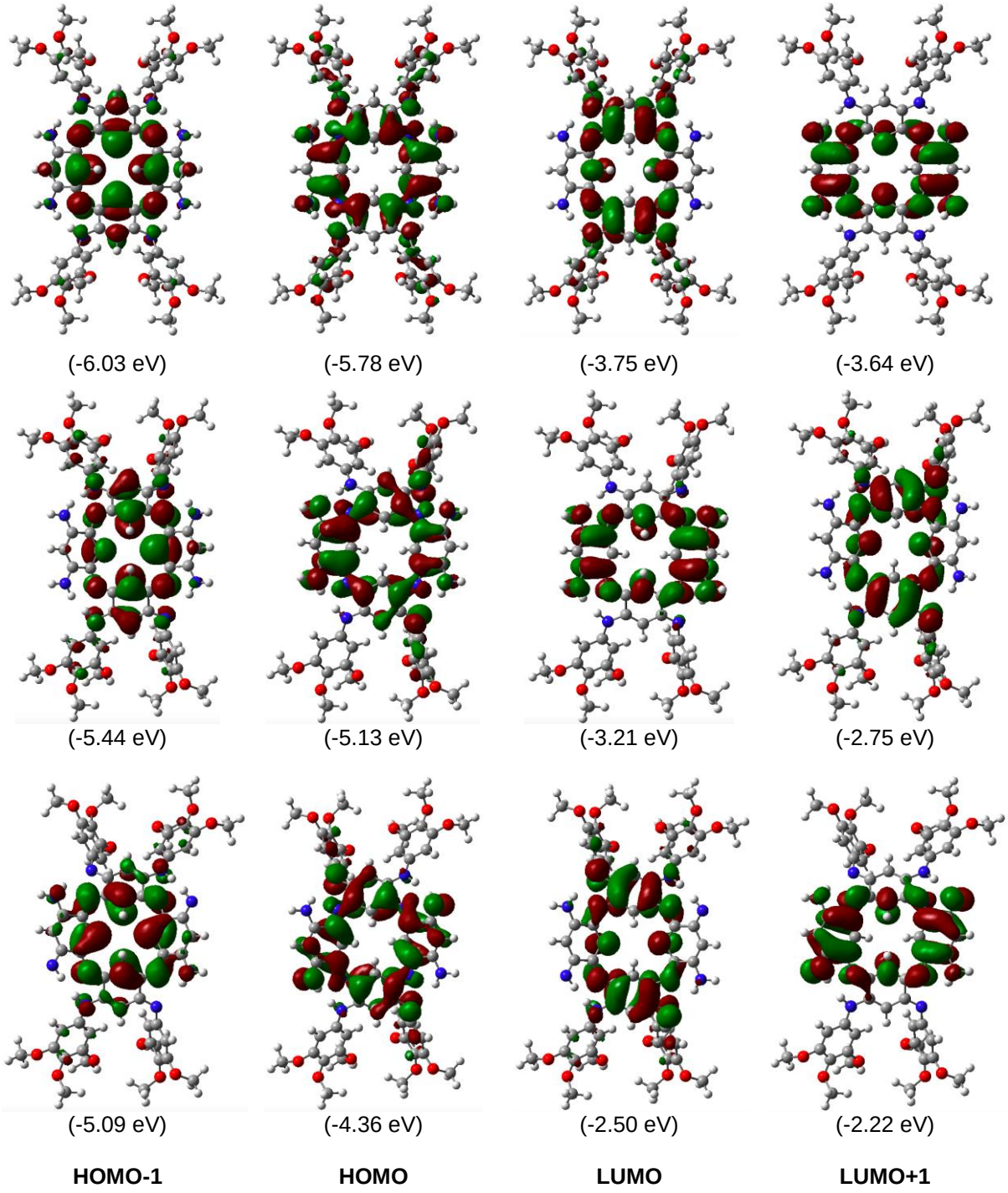

Figure S32. Representation of the four frontier MOs of (from top to bottom) **3a•2H$^+$**, **3a** and **3a**-**2H$^+$**.

S-IV. REFERENCES

1 K. N. Raymond, *Chem. Eng. News*, 1983, **61**, 4.
2 P. Gans and B. O'Sullivan, *Talanta*, 2000, **51**, 33-37.
3 (a) H. Gampp, M. Maeder, C. J. Meyer and A. D. Zuberbühler, *Talanta*, 1985, **32**, 95-101; (b) F. J. C. Rossotti, H. S. Rossotti and R. J. Whewell, *J. Inorg. Nucl. Chem.*, 1971, **33**, 2051-2065; (c) H. Gampp, M. Maeder, C. J. Meyer and A. D. Zuberbu¨hler, *Talanta*, 1985, **32**, 257-264; (d) H. Gampp, M. Maeder, C. J. Meyer and A. D. Zuberbühler, *Talanta*, 1986, **33**, 943-951.
4 (a) D. W. Marquardt, *J. Soc. Ind. Appl. Math.*, 1963, **11**, 431-441; (b) M. Maeder and A. D. Zuberbuehler, *Anal. Chem.*, 1990, **62**, 2220-2224.
5 L. Alderighi, P. Gans, A. Ienco, D. Peters, A. Sabatini and A. Vacca, *Coord. Chem. Rev.*, 1999, **184**, 311-318.
6 L. Lavaud, Z. Chen, M. Elhabiri, D. Jacquemin, G. Canard and O. Siri, *Dalton Trans.*, 2017, **46**, 12794-12803.
7 Z. Chen, R. Haddoub, J. Mahé, G. Marchand, D. Jacquemin, J. Andeme-Edzang, G. Canard, D. Ferry, O. Grauby, A. Ranguis and O. Siri, *Chem. Eur. J.*, 2016, **22**, 17820-17832.
8 M. J. Frisch, et al. Gaussian 16, revision A.03, Wallignford, CT, USA, **2016**.
9 C. Adamo and V. Barone, *J. Chem. Phys.* 1999, **110**, 6158-6169.
10 J. Tomasi, B. Mennucci and R. Cammi, *Chem. Rev.* 2005, **105**, 2999-3093.